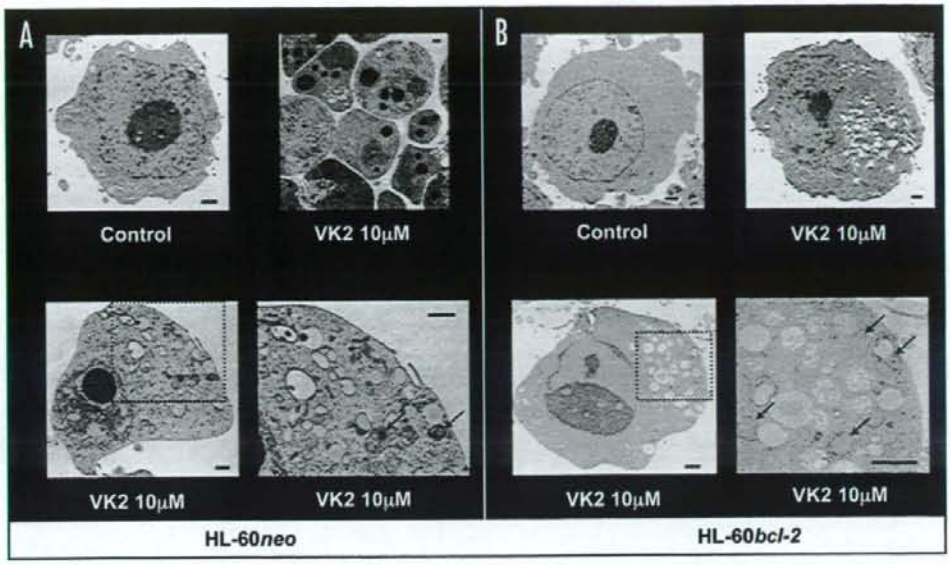


Figure 2. Ultrastructural features of HL-60*neo*/HL-60*bcl-2* cells after exposure to VK2. HL-60*neo*/HL-60*bcl-2* cells treated with or without 10 μM of VK2 for 72 hr. Then the cells were fixed, and the electron microscopy was performed. (A) HL-60*neo* cells: upper left; untreated control cells, upper right and lower; VK2-treated cells. (B) HL-60*bcl-2* cells: upper left; untreated cells, upper right and lower; VK2-treated cells. Arrows indicate autolysosomes.

vesicular organelles (AVOs) with acridine orange staining followed by flow cytometry as previously reported.[29] Figure 3C demonstrates that treatment with 10 μM VK2 increased the bright red fluorescence intensity (y-axis) from 4.8% to 46.8% in HL-60*neo* cells and that from 4.7% to 47.3% in HL-60*bcl-2* cells, respectively. These data further support the conclusion that autophagy is induced as well as apoptosis in HL-60*neo* cells. By increasing the concentration of VK2 at 20 μM, the intensity of AVO decreased to 31.5% in HL-60*neo* cells, indicating suppression of autophagy. Under these conditions apoptosis masked autophagy by inducing rapid cell death.

Additionally, LC3 protein is known to exist in two cellular forms such as LC3-I and LC3-II. LC3-I is converted to LC3-II by conjugation to phosphatidylethanolamine, and the amount of LC3-II is a good early marker for the formation of autophagosomes.[36,37] During 96 hr exposure to VK2, we analyzed the amount of LC3-II and also assessed the cleaved forms of caspase-3 as marker for apoptosis in HL-60*neo*/*bcl-2* cells. In HL-60*neo* cells, the amount of LC3B-II increased within 48 hrs of exposure to VK2. In HL-60 *bcl-2* cells the amount of LC3B-II was detected after 72–96 hr exposure to VK2 (Fig. 3D). In addition, recent evidence suggests that the accumulation of LC3-II is more accurately represented in autophagic flux in the presence of lysosomal inhibitors.[38] In the presence of E-64-d and pepstatin A, endogenous LC3B-II increased after treatment with VK2 in both HL-60*neo* and HL-60*bcl-2* cells (Fig. 3E). Immunoblotting with anti-caspase-3 mAb revealed that the cleaved form of caspase-3 was significantly increased after treatment with VK2 for 48–96 hr in HL-60*neo* cells, whereas the cleaved caspase-3 was almost undetectable in HL-60*bcl-2* cells during the 96 hr-exposure to VK2 (Fig. 3D). These results demonstrated that both autophagy and apoptosis occurred at the same time in HL-60*neo* cells. In addition, autophagy was induced earlier in HL-60*neo* cells than in HL-60*bcl-2* cells during exposure to VK2. This was further confirmed by electron microscopy of HL-60*neo* cells without nuclear fragments but with chromatin condensation after treatment with VK2, which may represent the earlier phase of apoptosis. These cells showed autophagosomes and autolysosomes in the cytoplasm (Fig. 2A; lower). Interestingly, some HL-60*bcl-2* cells with chromatin condensation also showed autophagosome formation (Fig. 2B; lower).

All data shown above indicated that autophagy can be induced both in HL-60*neo* and HL-60*bcl-2* cells in response to VK2, but it becomes more prominent in HL-60*bcl-2* cells because the cells are protected from rapid apoptotic cell death after 96 hr-treatment with VK2. In addition, HL-60*neo* cells undergo both autophagy and apoptosis. To confirm this evidence, we further examined the effect of Z-DEVD-FMK, a caspase-3 inhibitor, in HL-60*neo* cells. HL-60*neo* cells were cultured with Z-DEVD-FMK at various concentrations with/without 10 μM VK2. As shown in Figure 4A, cell growth inhibition by VK2 was attenuated in the presence of 10 μM and 100 μM of Z-DEVD-FMK. Z-DEVD-FMK alone at these concentrations did not show any cytotoxic effect during 96 hr-exposure. Then, HL-60*neo* cells were treated with VK2 with/without 100 μM of Z-DEVD-FMK for the assessment of autophagy induction. Since many cells were lost via apoptosis during 96 hr-exposure to VK2 without Z-DEVD-FMK, cellular proteins were lysed and protein contents were equalized for immunoblottings. Z-DEVD-FMK showed significant inhibition of VK2-induced caspase-3 activation as assessed by capsease-3 cleavage. Notably, autophagy induction assessed by LC3B-II formation was significantly enhanced in the presence of Z-DEVD-FMK after 96 hr exposure to VK2 (Fig. 4B). These data also supported that autophagy becomes more prominent by blocking apoptotic cell death.

**Mixed morphologic feature of autophagy and apoptosis in HL-60*bcl-2* cells.** The data shown above led us to further examine the morphologic features of HL-60*bcl-2* and HL-60*neo* cells in detail after exposure to VK2.

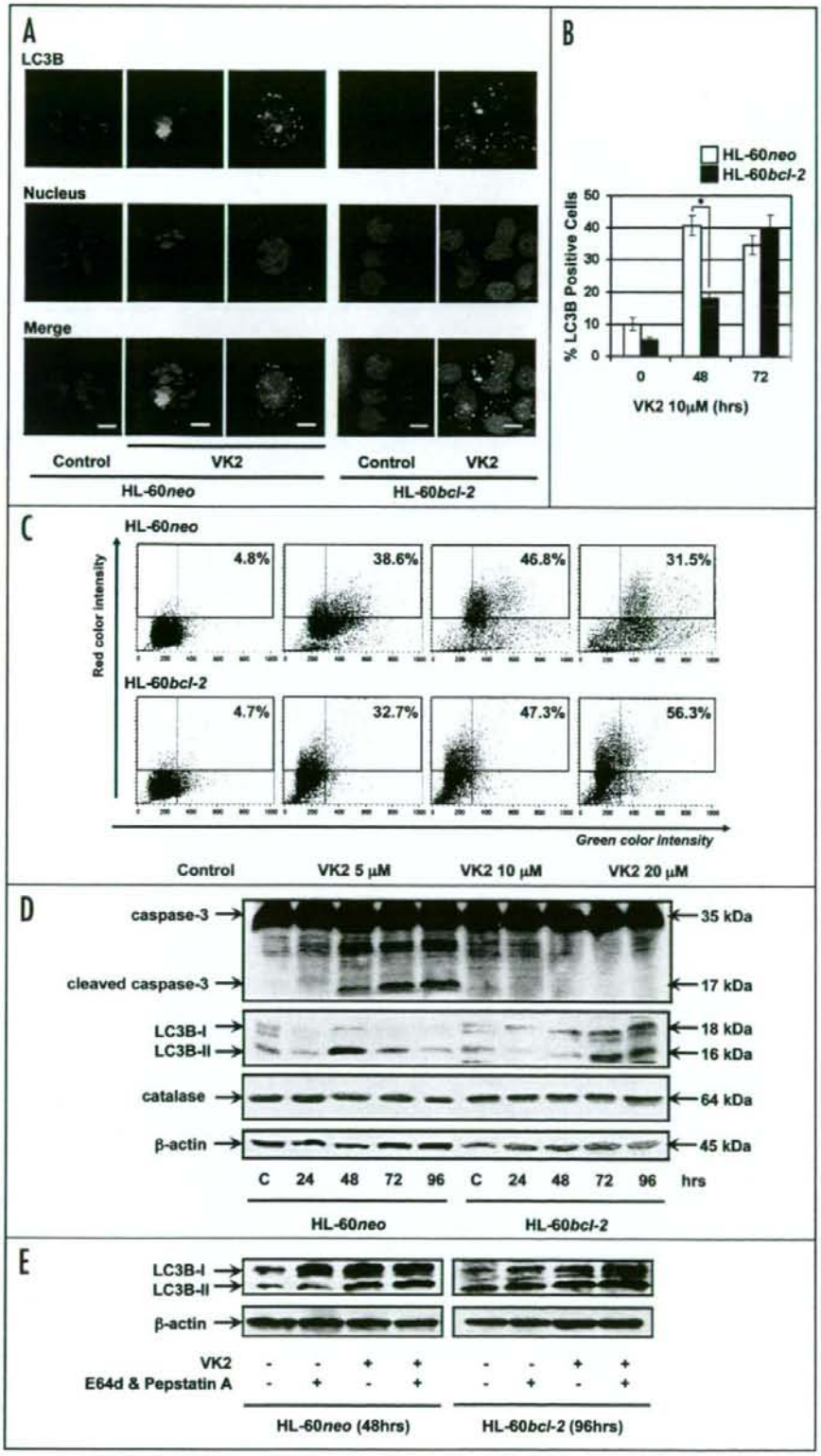


Figure 3. Induction of autophagy in response to VK2 in HL-60*neo*/HL-60*bcl-2* cells. *Involvement of LC3B in VK2-induced autophagy:* After exposure to 10 μM VK2 for 48 and 72 hr, the cells were processed for fluorescent immunocytostaining with anti-LC3B Ab and counterstaining with DAPI for nucleus as described in Materials ant Methods. (A) HL-60*neo*/*bcl-2* cells (original magnification x 1,000). (B) Quantification of the cells showing the punctuated pattern of LC3B staining, which marks cells with autophagosome formation. One hundred cells were assessed and ratios for the cells showing the punctuated pattern of LC3B staining were expressed. Results shown are the means ± SD from the results of three independent experiments. *$p < 0.001$. *Development of acidic vesicular organelles (AVOs) after VK2 treatment:* (C) After staining the cells with acridine orange, AVOs were quantified using flowcytometer in HL-60*neo* (upper) and HL-60*bcl-2* (lower) treated with or without VK2 (5 μM, 10 μM or 20 μM) for 72 hr. X-axis, green color intensity; Y-axis, red color intensity. *Expression of isoforms of LC3B and caspase-3:* (D) Cellular proteins were lysed at the indicated time after incubation with or without 10 μM of VK2. Proteins were separated by either 11.25% or 15% SDS-PAGE. Aliquots of 40 μg of protein extracts were used for immunoblotting using anti-caspase-3 and anti-LC3B Abs, respectively. The anti-β-actin mAb was used for protein-loading equivalence. *Expression of isoforms of LC3B in the presence and absence of protease inhibitors:* (E) After treatment with 10 μM of VK2 for 44 hrs in HL-60*neo* and for 92 hrs in HL-60*bcl-2* cells, cells were further cultured with/without protease inhibitors, E-64-d (10 μg/ml) and pepstatin A (10 μg/ml) in the presence of VK2 for 4 hrs. Cellular proteins were lysed and immunoblotted with anti-LC3B Ab.

After exposure to VK2 for 96 hr, HL-60*bcl-2* cells showed an increased percentage of fragmented nuclei compared to 72 hr treatment. Intriguingly, the morphologic findings in HL-60*bcl-2* cells undergoing apoptosis were different from those in HL-60*neo* cells; each nuclear fragment appeared to be encapsulated by vesicles resulting in the formation of a "sunny side-up" appearance (Fig. 5A). A "sunny side-up" appearance was also observed in HL-60*neo* cells treated with VK2 in the presence of a caspase-3 inhibitor, Z-DEVD-FMK. Extended exposure to VK2 up to 6 days resulted in the disappearance

of this characteristic feature and the appearance of the typical apoptotic bodies like in HL-60*neo* cells treated with 72 hr exposure to VK2 (Fig. 5B). Therefore, this morphologic change in HL-60*bcl-2* cells seems to be an early phase of cells undergoing apoptosis. To investigate whether the "sunny side-up" feature is macroautophagy of nuclear fragments, we examined the VK2 treated HL-60*bcl-2* cells by electron microscopy. Fragmented nuclei with condensed chromatin appeared to be surrounded by double-membrane (Fig. 5C). However, fluorescent immunocytostaining with anti-LC3B Ab showed that nuclear fragments were not surrounded by punctuated LC3B. Therefore, "sunny side-up" feature does not appear to represent the macroautophagy of nuclear fragments.

**The biological roles of VK2-induced autophagy in HL-60*neo/bcl-2* cells.** Since autophagy was initially recognized as a cellular survival process under amino acid starvation,[23,24] the concept of autophagic cell death as type II PCD and the significance of cancer treatment-induced autophagy is a subject of debate. Autophagy may function as an anti-cancer effect or a cytoprotective reaction against the cytotoxic reagents.[20-22] To assess the role of VK2-induced autophagy in HL-60 cells, we attempted to block the autophagic process in the presence or absence of VK2 using 3-MA, an inhibitor of class III phosophatidyl-inositol-3 kinase (PI3K),[31] and siRNA against Atg7, respectively. Treatment with 3-MA suppressed the PI-staining positive cells in HL-60*neo/bcl-2* cells treated with VK2. 3-MA alone showed no effect on HL-60 cell growth. In addition, the decreased viability of HL-60*neo* and HL-60*bcl-2* cells after VK2 treatment was reversed in the presence of 3-MA (Fig. 6A and B). Furthermore, 3-MA suppressed the induction of AVOs in HL-60*neo/bcl-2* cells treated with VK2 (Fig. 6C). siRNA effectively suppressed Atg7 expression in HL-60neo/*bcl-2* cells. Suppression of Atg7 resulted in significant attenuation of cell growth inhibition by VK2 in both cell lines (Fig. 6D). All these data support the conclusion that autophagic cell death was induced after treatment with VK2. To further confirm this interpretation, we used the Tet-off system with an Atg5$^{-/-}$ mouse embryonic fibroblast (MEF) cell line.[33] Pretreatment of Tet-off Atg5$^{-/-}$ MEF cells with 10 ng/ml doxycycline hydrochloride (Dox) for 120 hrs induced complete suppression of Atg5 expression. Thereafter, the cells were further cultured in the presence or absence of VK2 for 72 hrs. As shown in Figure 7, the VK2- induced cell growth inhibition at 10 μM was significantly attenuated in Dox treated-MEF cells along with suppression of the induction of LC3B-II. These data also support the occurrence of autophagic cell death in response to VK2.

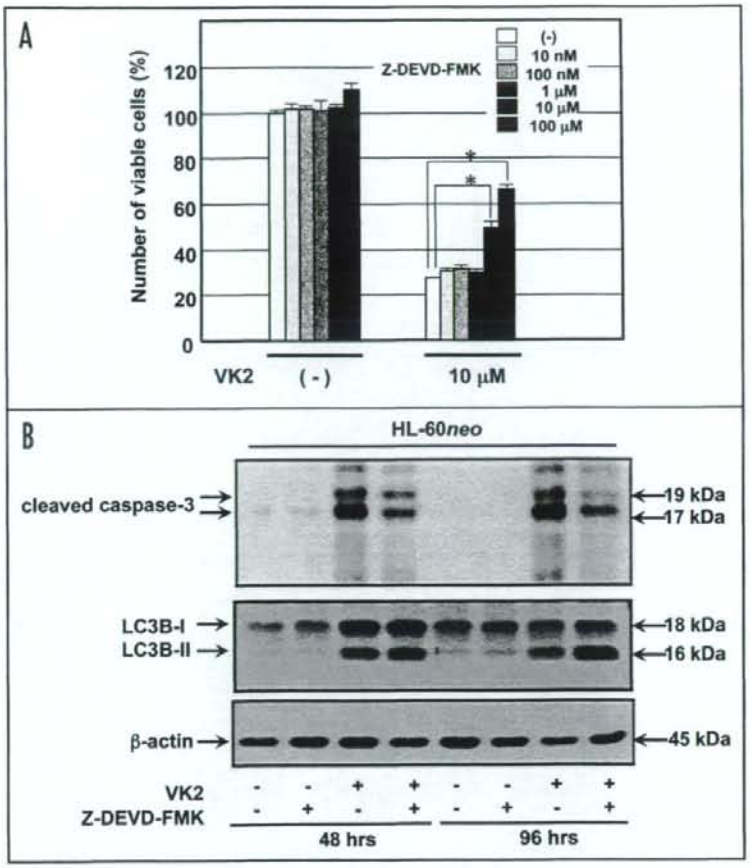


Figure 4. Effects of a caspase-3 inhibitor on VK2-induced autophagy in HL-60*neo* cells. (A) HL-60*neo* cells were cultured with Z-DEVD-FMK at various concentrations with/without 10 μM of VK2 for 96 hr. The number of cells was assessed with the WST cell counting kit as described in Materials and Methods. *$p < 0.001$. (B) HL-60*neo* cells were treated with 10 μM VK2 with/without 100 μM of Z-DEVD-FMK for 48 hr and 96 hr, respectively. Cellular proteins were lysed and separated by either 11.25% or 15% SDS-PAGE. Aliquots of 40 μg of protein extracts were used for immunoblotting using anti-cleaved caspase-3 Ab, anti-LC3B Ab, and anti-β-actin mAb, respectively.

## Discussion

In the present study, we demonstrated that VK2 induces autophagy as well as apoptosis in HL-60 cells. In addition, the mixed morphologic features of apoptosis and autophagy such as chromatin condensation and fragmented nuclei for apoptosis and autophagosomes and autolysosomes for autophagy were detected in the same cells (Fig. 2A and B). This suggests that the cellular processes for apoptosis and autophagy are simultaneously induced in response to VK2 as well as some previous reports in Drosophila and sympathetic neurons.[39,40] Immunoblottings for LC3B and caspse-3, which were performed for assessment of autophagy and apoptosis induction, also support this evidence (Fig. 3D). During extended exposure to VK2 in cells with higher expression of Bcl-2, autophagy became more evident, because cells with lower expression of Bcl-2 underwent apoptotic cell death and were eliminated from culture system. This indicates that the cellular expression levels of Bcl-2 appear to determine the phenotype of cell death. Induction of autophagy in cancer cells in response to various anti-cancer reagents has been reported: Temozolomide (TMZ), a DNA alkylating agent, and arsenic trioxide

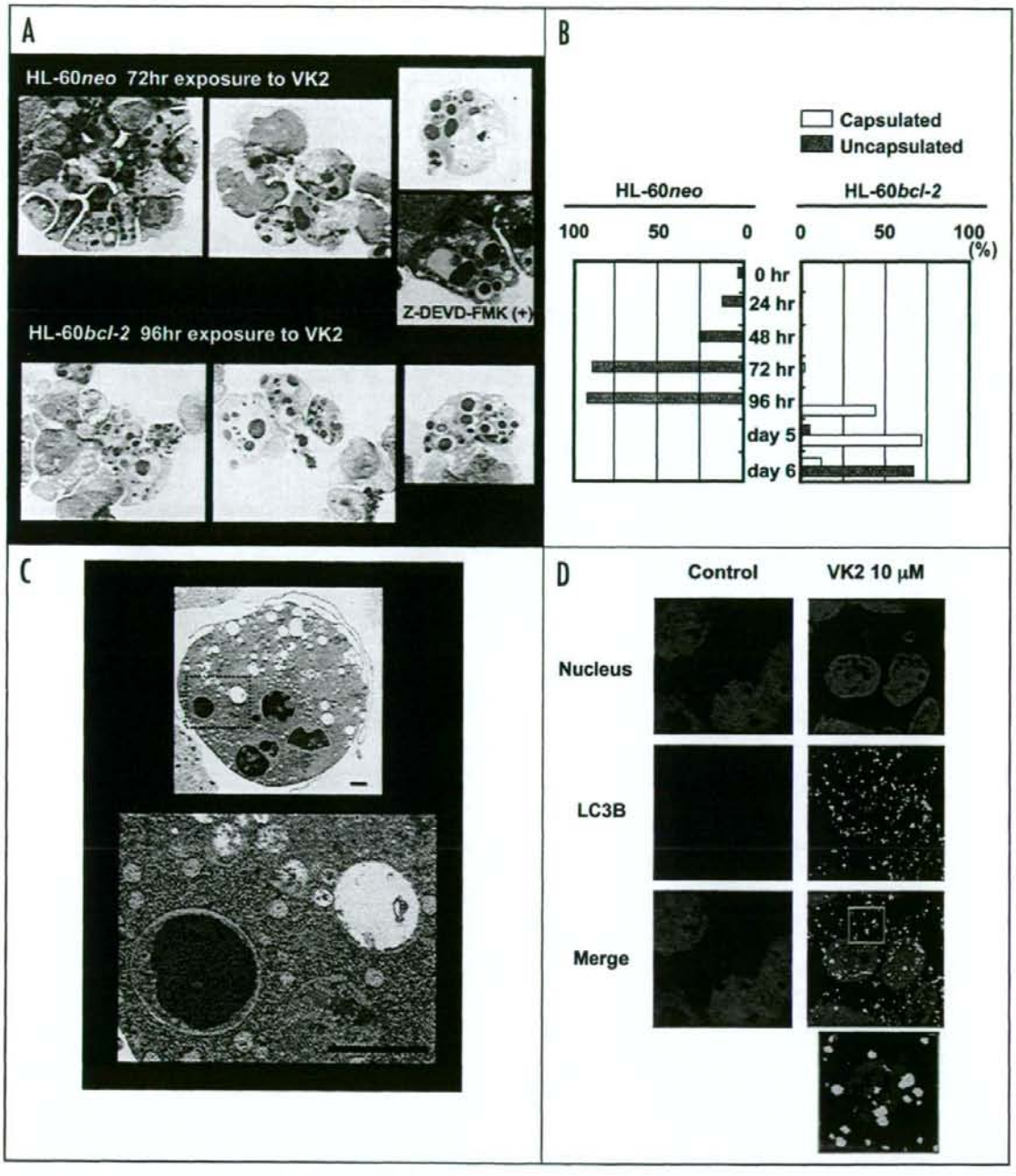


Figure 5. Capsulated fragmented nuclei in HL-60*bcl-2* cells after treatment with VK2. (A) Morphological features of HL-60*neo* after 72 hr-treatment with VK2 (10 μM) with/without Z-DEVD-FMK (100 μM) and of HL-60*bcl-2* cells after 96 hr-treatment with VK2. May-Grünwald-Giemsa staining, original magnification x 1,000. (B) Percentages of HL-60 cells with apoptotic bodies containing either capsulated nuclear fragments or uncapsulated nuclear. After treatment HL-60*neo/bcl-2* cells with 10 μM of VK2 for various length of time, morphologic changes were assessed in 100 cells after May-Grünwald Giemsa stain as well as Figure 4A. (This is one of representative result from 3 separate experiments.) (C) Electron microscopy of HL-60*bcl-2* cells after treatment with 10 μM VK2 for 96 hr. (D) Fluorescent immunocytostaining with anti-LC3B Ab in HL-60*bcl-2* cells after 96 hr-treatment with 10 μM VK2. Fluorescent immunocytostaining with anti-LC3B Ab (original magnification x 1,000) was performed as described in Figure 3A and C, respectively. The slides stained with anti-LC3B Ab were monitored using Zeiss LSM510 confocal microscope (Original magnification x 600).

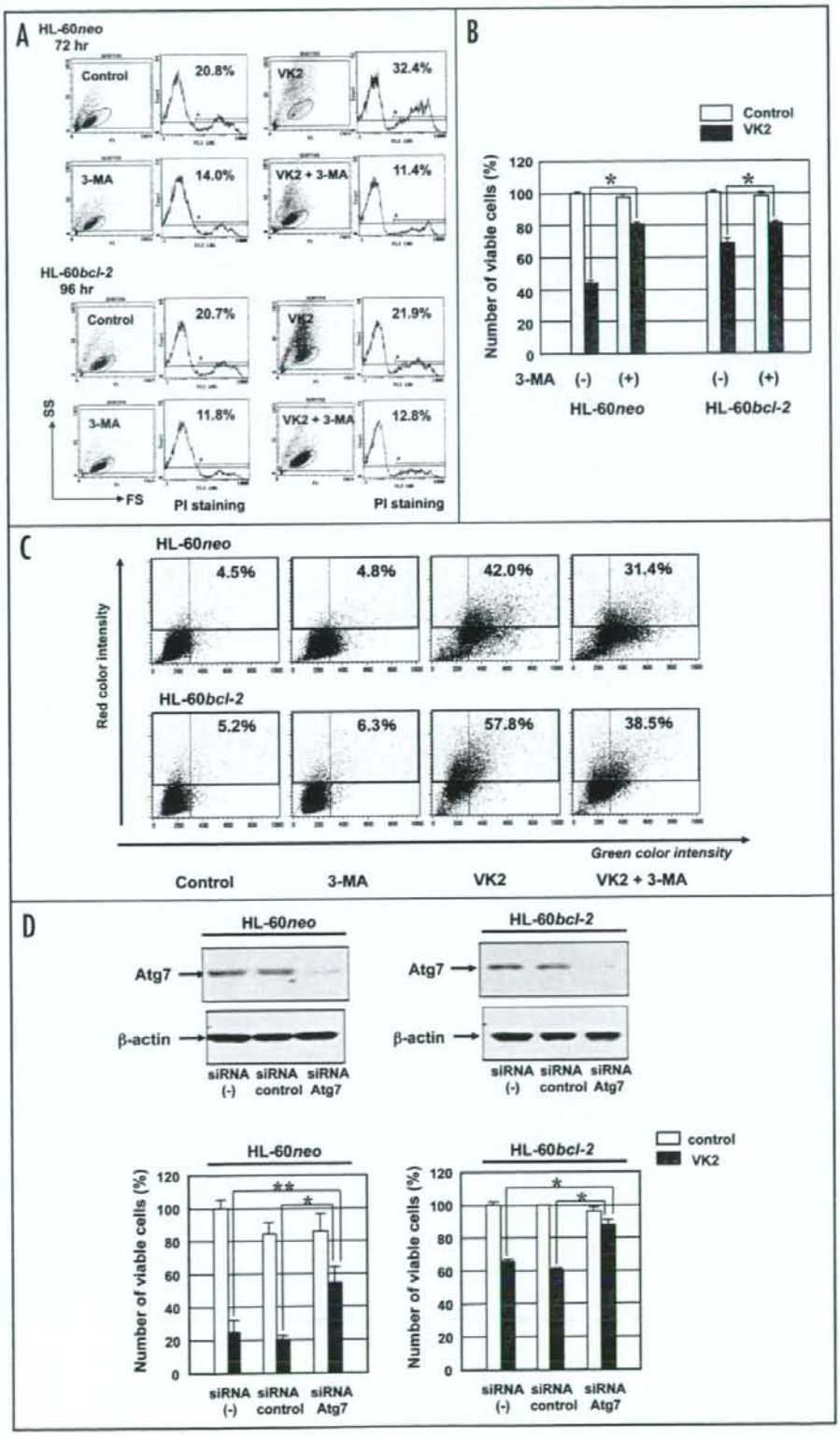


Figure 6. Effects of inhibition of VK2-induced autophagy in HL-60*neo*/*bcl-2* cells. (A and B) To inhibit autophagy, 2 mM 3-MA was added to HL-60 cell cultures for 72 hr with or without VK2. Viable cell numbers were assessed using a flow cytometer as described in Materials and Methods. *p < 0.001 (C) Treatment with 3-MA suppressed the induction of acidic vesicular organelles (AVOs) in HL-60*neo*/*bcl-2* cells treated with 10 μM of VK2. AVOs were quantified with fluorescence-activated cell sorter in HL-60*neo* (upper)/HL-60*bcl-2* (bottom). x-axis, green color intensity; y-axis, red color intensity. (D) Inhibition of Atg7 protein expression by siRNA transfection: HL-60neo/*bcl-2* cells were transfected with random siRNA or siRNA for Atg7 for 72 hrs. Relative expression levels of Atg7 proteins were assessed by western blotting. (upper). After treatment with/without random siRNA or siRNA for ATG7, the cells were further treated with VK2 for 72 hrs. Thereafter, cell growth inhibition was assessed by WST cell counting kit (lower). *p < 0.001, **p < 0.05.

($As_2O_3$) induce autophagy of malignant glioma cells, which are usually refractory to various anti-cancer therapies.[30,41] The histone deacetylase inhibitors sodium butyrates and suberoylanilide hydeoxamic acid (SAHA) induce autophagic cell death in HeLa cells which overexpress the anti-apoptotic protein Bcl-$X_L$, but they induce apoptosis in parental HeLa cells.[42] Murine L929 fibroblastic cells, murine RAW 264.7 macrophages, and human U937 leukemia cells underwent autophagy after treatment with z-VAD-fmk, a pancaspase inhibitor.[43] Etoposide induces autophagic cell death in Bax/Bak-double knockout MEF, and these cells also undergo protective autophagy under conditions of nutrition depletion.[44] These conditions for induction of autophagy by cytotoxic stimuli include cellular resistance against apoptosis or protection from apoptosis. Our observations showing autophagy in HL-60*bcl-2* rather than HL-60*neo* cells meet these conditions. However, our data also demonstrated that apoptotic and

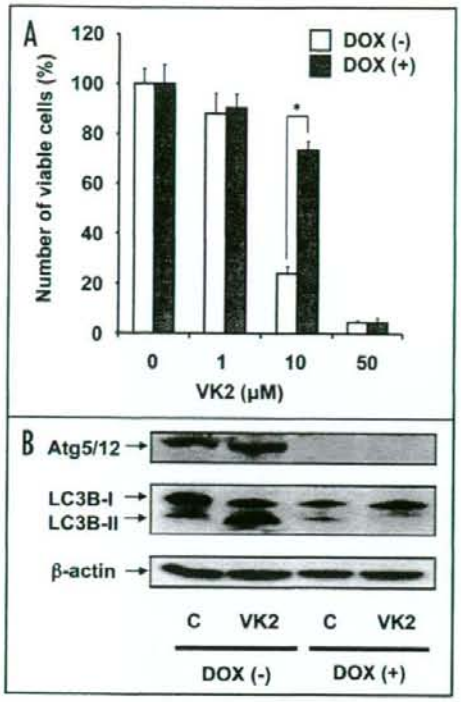


Figure 7. Effects of inhibition of VK2-inducing autophagy in a Atg5$^{-/-}$ mouse embryonic fibroblast (MEF) cell line with the Atg5 Tet-off system. Tet-off Atg5 MEF cells were incubated with 10 ng/ml doxycycline hydrochloride (Dox) for 120 hrs, and thereafter cultured in the presence or absence of 1 to 50 μM of VK2 for 72 hrs. (A) Cell growth inhibition in response to VK2 was assessed using WST assay kit. (B) MEF cells treated with or without Dox were cultured in the presence or absence of 10 μM of VK2 for 72 hr. Then, cellular proteins were separated by 11.25% SDS-PAGE and immunoblotted with either anti-Atg5, anti-LC3B, or anti-β-actin Abs.

autophagic processes can be simultaneously induced by VK2 (Figs. 2 and 3).[39,40] Therefore, cell death induced by cytotoxic reagents cannot be simply characterized in stereotyped manner such as type I PCD versus type II PCD.

Although autophagy became evident in HL-60*bcl-2* cells, previous reports have demonstrated that Bcl-2 negatively regulates induction of autophagy. Bcl-2 localized on endoplasmic reticulum was reported to interact with Beclin 1 and to inhibit Beclin 1-dependent autophagy.[27] This anti-autophagy function of Bcl-2 was suggested to help maintain autophagy at the levels that are compatible with cell survival, rather than cell death.[27] In addition, downregulation of Bcl-2 by the conditional expression of the full length bcl-2 antisense message was reported to induce autophagic cell death in HL-60 cells,[26] and Bcl-2/Bcl-$X_L$ antagonist HA14-1 also induces autophagy and apoptosis in L1210 murine leukemia cells,[45] suggesting anti-autophagic function of Bcl-2. In our data, comparing autophagy induction between HL-60*neo* and HL-60*bcl-2* by the formation of punctuated LC3B, autophagy was rather enhanced in HL-60*neo* cells within 72 hrs of exposure to VK2 (Fig. 3B). Delayed induction of autophagy in HL-60*bcl-2* as assessed by conversion of LC3B type I to type II was also observed (Fig. 3D). These data agree with previous reports that Bcl-2 has a negative effect on the induction of autophagy. However, since *bcl-2* knockout mice are viable with almost intact bone marrow functions,[46] other regulatory pathway(s) might be involved for autophagy, especially when the cells are exposed to cytotoxic reagents. It has been reported that intracellular calcium mediates the induction of autophagy in a Bcl-2 regulated fashion.[47] These findings raise the question as to how a cell decides to undergo either apoptosis or autophagy in response to calcium signals.

It was intriguing that some morphologic features of the same death pathway differed between HL-60*neo* and HL-60*bcl-2* cells. As shown in Figure 5A and B, nuclear fragments were capsulated in HL-60*bcl-2* cells but not in HL60*neo* cells. Longer exposure to VK2 resulted in disappearance of this "sunny side-up" feature which seems to detect an early phase of apoptosis. These encapsulated nuclear fragments should be designated as "apoptotic bodies" as in previous reports.[48] The formation of "sunny side-up" may be only detectable under conditions for autophagy inductions along with a higher threshold for apoptosis such as overexpression of anti-apoptotic Bcl-2 proteins or in the presence of a caspase-3 inhibitor. However, we could not prove the macroautophagy formation of fragmented nuclei by LC3B fluorescence immunocytostaining (Fig. 5D) Biological significance of this distinct phenomenon remains to be cleared.

Although "autophagic cell death" has recently been clearly demonstrated in salivary gland cells during development of Drosophila,[49] the concept of autophagy as type II PCD is still controversial, especially the cell death induced by anti-cancer reagents.[20-22] In the presence of 3-MA, an inhibitor of type III PI3K, VK2-induced cell death was significantly suppressed not only in HL-60*bcl-2* but also in HL-60*neo* cells (Fig. 6A–C). This suggests that the VK2-induced autophagy induces cell death. However, 3-MA is not a specific inhibitor for autophagy and it may interact with other signaling pathways for cell death.[22,37] Knockdown of Atg7 with siRNA prevented VK2-induced cell death (Fig. 6D). Tet-off Atg5 MEF system also demonstrated an attenuation of VK2-induced cell growth inhibition along with inhibition of autophagy (Fig. 7). Therefore, the enhanced autophagy in response to VK2 is correlated with induction for cell death in our system. These lines of evidence strongly suggest "autophagic cell death" or "autophagy medicated cell death" in leukemia cells. However, the executor(s) for induction of cell death still remains to be cleared. Yu Li et al., reported that caspase inhibition leading to cell death by means of autophagy involves accumulation of reactive oxygen species (ROS), membrane lipid oxidation, and loss of plasma membrane integrity in L929 cells.[50] The accumulation of abnormal ROS was caused by the selective autophagic degradation of the catalase, which is the major enzymatic ROS scavenger.[50] The accumulation of ROS following degradation of catalase might be one of the executors of autophagic cell death when caspases are inhibited. However, as shown in Figures 1A and 3D, catalase expression was not different between HL-60*neo* and HL-60*bcl-2* cells, and no significant change of catalase expression during 96 hr exposure to VK2. Therefore, our observation cannot be explained by degradation of catalase. In fat body cells and wing discs of Drosophila, overexpression of Atg1 itself was sufficient to induce autophagy along with apoptosis in a caspase-dependent manner.[40] This suggests that autophagy represents an alternative induction of apoptosis rather than a distinct form of cell death. In contrast, autophagy is activated by apoptotic signaling in sympathetic neurons.[39] In this system, the same apoptotic signal induces

mitochondrial dysfunction and also activates autophagy. Once it was activated, autophagy was suggested to mediate caspase-independent neuronal death.[39] It is noteworthy that knockdown of Atg7 using siRNA as well as 3-MA treatment showed attenuation of growth inhibition by VK2 in HL-60*neo* cells (Fig. 6D). Since apoptotic cell death should be dominant in HL-60*neo* cells, autophagy may function as an alternative inducer for apoptosis. This may be further supported by the distinct morphologic change in some but not all HL-60*bcl-2* cells after longer exposure to VK2, which showed apoptotic bodies with "sunny side-up" feature (Fig. 4A and B).

Qu X et al., demonstrated that autophagy contributes to the clearance of dead cell by a mechanism that likely involves the generation of energy-dependent engulfment signals.[51] This suggests an extended role for autophagy in the disposal of dead cells by a phagocytic system in vivo. Although this novel function of autophagy for PCD was demonstrated in ES cells during embryonic development, it may also extend to cancer cells. Autophagy induction in response to VK2 may explain the selective clearance of a leukemic clone via the phagocytic system in vivo.[2,6,11] Autophagy induction by VK2 shown in this study may give us novel therapeutic tools in the treatment of leukemia.

## Materials and Methods

**Cell lines and reagents.** HL-60 cells obtained from the American Type Culture Collection (Rockville, MD) were maintained in continuous culture in RPMI 1640 medium (GIBCO, Grand Island, NY) supplemented with 10% FCS (Hyclone, Logan, UT), 2 mM L-glutamine, penicillin (50 U/ml), and streptomycin (100 μg/ml). A clone stably transfected with the human *bcl-2* gene, HL-60*bcl-2*, was established by electroporation using a recombinant pdDNA3-plasmid-containing the human *bcl-2a* gene.[26] HL-60*neo* is a control cell line transfected with pdDNA3-plasmid alone.[26] VK2 (menaquinon-4) was supplied by Eisai Co., Ltd. (Tokyo, Japan). E-64-d and Pepstatin A, which are inhibitors for lysosomal proteases, were purchased from BIOMOL International L.P. (Plymouth Meeting, PA). Z-DEVD-FMK for a caspase-3 inhibitor was purchased from R & D Systems Inc. (Minneapolis, MN).

**Assessment of viable cell count.** HL-60 cells treated with or without VK2 were stained with a solution containing 1% (v/v) propidium iodide (PI) (Sigma-Aldrich, St. Louis, MO) for 30 min at 4°C. First, the gating area of cytogram for detecting viable HL-60 cells was established according to both the PI staining-negative area (indicating viable cells) and the forward- and side- scatter intensities.[2] Then the cell cultures were pipetted gently to obtain uniform cell suspension, and were introduced to a flow cytometer. The number of cells in gating area for viable HL-60 cells was assessed for 60 sec. The number relative to the cells treated with control medium revealed to be well-correlated with the results obtained from a WST Cell Counting Kit (Dojin East, Tokyo, Japan), with absorption measurements at 450 nm.[2] In some experiments viable cell counts were assessed by trypan blue dye exclusion.

**Quantitative detection of acid vesicular organelles (AVOs) with acridine orange staining.** Autophagy is the process of sequestrating cytoplasmic proteins and organelles into the lysosomal component and characterized by development of AVOs. To detect and quantify AVOs in VK2-treated cells, we performed vital staining with acridine orange (Polysciences, Warrington, PA) as described previously.[29,30] To inhibit autophagy 2 mM 3-methyladenine (3-MA) (Polysciences Inc, Warrington, PA), an inhibitor of the phosphatidylinositol 3-kinase (PI3K),[31] was added to the cultures for 72 hr with/without VK2. HL-60 cells were stained with 1.0 μg/ml acridine orange for 15 min at room temperature and processed for flow cytometry using the FACScan Cytometer (Becton Dickinson, San Jose, CA) and analyzed with CellQuest software (Becton Dickinson).

**Immunoblotting.** Cells were lysed in Lysis Buffer (10 mM Tris-HCL PH 7.8, 150 mM NaCl, 1% NP-40, 1 mM EDTA, 10% glycerol, 1 mM phenylmethylsulfonyl fluoride, 0.15 U/ml aportinine, 10 mg/ml leupeptine, 100 mM sodium fluoride, 2 mM sodium orthovanadate ), and cellular proteins were quantified using the Protein Assay kit of Bio-Rad (Richmond, CA). Equal amounts of proteins were loaded, separated by SDS-PAGE and transferred onto Hybond-P membranes (Amersham Biosciences Corp., Piscataway, NJ). The membranes were probed with antibodies (Abs) such as anti-human Bcl-2 monoclonal (m) Ab (BD Biosciences Pharmingen, San Jose, CA), anti-microtubule-associated protein 1 light chain 3B (LC3B) Ab, anti-caspase-3 Ab (Cell Signaling Technology, Danvers, MA), anti-cleaved caspase-3 Ab (Cell Signaling Technology), anti-Atg5 Ab (Abgent, San Diego, CA), anti-Atg7 Ab (ProSci, Poway, CA), anti-human catalase rabbit mAb (Epitomics Inc., Burlingame, CA), and anti-β-actin Ab (Sigma-Aldrich), respectively. Anti-LC3B Ab was generated as previously described.[32] Immunoreactive proteins were detected by horseradish peroxidase-conjugated second Ab and an enhanced chemiluminescence reagent (ECL) (Amersham Biosciences Corp.).[3]

**Assessment of apoptosis.** Apoptosis was detected by morphology, flow cytometry using Annexin V-florescein isothiocyanate (FITC) apoptosis detection kit I (BD Biosciences, San Diego, CA), and by immunoblotting with either anti-caspase-3 or anti-cleaved caspase-3 Abs as described above. For flow cytometry, HL-60 cells treated with or without VK2 were washed twice with ice cold phosphate-buffered saline and then resuspended in 1 X binding buffer (1 x $10^6$ cells/ml). 100 μl of cell suspension (1 x $10^5$ cells) was then transferred to a 5 ml tube, and 5 μl of Annexin V-PE and 5 μl of 7-amino-actinomycin were added. After 15 min of incubation at room temperature in the dark, 400 μl of 1 X binding buffer was added and the tubes were analyzed in a FACScan instrument with CellQuest software (Becton Dickinson). For morphologic assessment for apoptosis, the cell suspension was sedimented in a Shandon Cytospin II (Shandon, Pittsburgh, PA), and preparations were stained with May-Grünwald-Giemsa and with 4'-6-diamidino-2-phenylindole (DAPI, Vector laboratories, Inc., Burlingame, CA).

**Measurement of mitochondrial membrane potential.** Mitochondrial membrane potential was measured with tetramethyl rhodamine ethyl ester perchlorate (TMRE: Molecular Probe Inc., Eugene, OR) using flow cytometry as described previously.[30] Cells were incubated with 150 nM TMRE at 37°C for 20 min in the dark and analyzed by FACScan using CellQuest software. The fluorescent dye TMRE is accumulated by mitochondria as a result of the mitochondrial membrane potential. Shift to the left in the emission spectrum indicates the depolarization of mitochondrial membrane potential in the apoptotic cells.

**Electron microscopy.** HL-60 cells were treated with/without VK2 and then fixed with a solution containing 3% glutaraldehyde plus 2% paraformaldehyde in 0.1 M cacodylate buffer (pH 7.3) for

1 hr. The samples were further post-fixed in 1% $OsO_4$ in the same buffer for 1 hr, and subject to the electron microscopic analysis using an electron microscope H-7000 (Hitachi, Tokyo, Japan) as described previously.[30] Representative areas were chosen for ultra-thin sectioning and viewed with an electron microscope.

**Fluorescent immunocytostaining.** Cells were fixed on glass slide by Shandon Cytospin II followed by further fixation with 4% paraformaldehyde for 20 min. After fixation, the cells on the slides were incubated with anti-LC3B Ab (1:5,000 dilution) in 0.5% Triton X-100-phosphate-buffered saline (PBS) overnight at 4°C. The slides were then washed with PBS and incubated with Alexa Fluor 488-labeled secondary goat anti-rabbit Ab (1:200 dilution) for 1 hr at room temperature. The slides were mounted with DAPI and monitored under an Axioskop 40 (Carl Zeiss MicroImaging, Inc., Thornwood, NY) or LSM 510 (Carl Zeiss MicroImaging).

**Small interfering RNA (siRNA) experiments.** siRNA oligonucleotides for human Atg7 (accession # NM-006395, catalog # L-020112), and siCONTROL non-targeting siRNA (catalog # D-001220) were purchased from GE Healthcare UK Ltd. (Buckinghamshire, England), and resuspended in RNase-free $H_2O$ at 20 μM. HL-60*bcl-2* cells were washed twice in serum-free media and resuspended to 1 x $10^7$ cells per 500 μl of cold, serum-free OPTI-MEM (GIBCO), and transferred to pre-chilled 0.4 cm-gap electroporation curettes (Bio-Rad). Cells were mixed with/without siRNA at 20 nM (final concentration) on ice for 5 min, thereafter, cells were pulsed once at 250 mV, 960 μF by using a Bio-Rad electroporator. The cell suspensions were then transferred to the incubator in 5% $CO_2$ at 37°C. Five hr after electroporation, the same volume of RPMI 1640 medium containing 20% FBS was added. Forty-eight hr after electroporation, protein knockdown was determined by immunoblotting, and the cells were treated with the indicated concentration of VK2 for 72 to 96 hr, and viable cells were assessed as previously described.

**Tet-off system with an Atg5$^{-/-}$ mouse embryonic fibroblasts (MEFs).** The Atg5 Tet-off MEF cell line was a kind gift from Dr Noboru Mizushima (Tokyo Medical and Dental University School of Health Science, Tokyo, Japan).[33] Atg 5 expression can be completely suppressed when this cell line is cultured in the presence of doxycycline. The culture condition is precisely described in elsewhere.[33]

**Statistics.** All data are given as the mean ± SD. Statistical analysis was performed by using Mann-Whitney's U test (two-tailed). The criterion for statistical significance was taken as $p < 0.05$.

**Acknowledgements**

We thank Ayako Hirota and Fumiko Komoda for their excellent technical assistance and Dr. Noboru Mizushima of Tokyo Medical and Dental University School of Health Science for a kind gift of the Atg5 Tet-off MEF cell line. We also thank Eisai Co. for providing menaquinone-4.

This study is supported by a Grant-in-Aid for Science Research (C) from the Ministry for Education, Science, Sports and Culture of Japan to K.M. (#18591089).

**References**

1. Lamson DW, Plaza SM. The anticancer effects of vitamin K. Altern Med Rev 2003; 8:303-18.
2. Yaguchi M, Miyazawa K, Katagiri T, Nishimaki J, Kizaki M, Tobyama K, Toyama K. Vitamin K2 and its derivatives induce apoptosis in leukemia cells and enhance of all-*trans* retinoic acid. Leukemia 1997; 11:779-87.
3. Yokoyama T, Miyazawa K, Yoshida T, Ohyashiki K. Combination of vitamin K2 plus imatinib mesylate enhances induction of apoptosis in small cell lung cancer cell lines. Int J Oncol 2005; 26:33-40.
4. Wang Z, Wang M, Finn F, Carr BI. The growth inhibitory effects of vitamins K and their actions on gene expression. Hepatology 1995; 22:876-82.
5. Otsuka M, Kato N, Shao RX, Hoshida Y, Ijichi H, Koike Y, Taniguchi H, Moriyama M, Shiratori Y, Kawabe T, Omata M. Vitamin K2 inhibits the growth and invasiveness of hepatocellular carcinoma cells via protein kinase A activation. Hepatology 2004; 40:243-51.
6. Miyazawa K, Aizawa S. Vitamin K2 improves the hematopoietic supportive functions of bone marrow stromal cells in vitro: a possible mechanism of improvement of cytopenia for refractory anemia in response to vitamin K2 therapy. Stem Cells Dev 2004; 5:449-51.
7. Miyazawa K, Nishimaki J, Ohyashiki K, Enomoto S, Kuriya S, Fukuda R, Horta T, Teramura M, Mizoguchi H, Uchiyama T, Omine M. Vitamin K2 therapy for myelodysplastic syndrome (MDS) and post-MDS acute myeloid leukemia: Information through a questionnaire survey of multi-center pilot studies in Japan. Leukemia 2000; 14:1156-7.
8. Yaguchi M, Miyazawa K, Otawa M, Ito Y, Kawanishi Y, Toyama K. Vitamin K2 therapy for a patient with myelodysplastic syndrome. Leukemia 1999; 13:144-5.
9. Habu D, Shiomi S, Tamori A, Takeda T, Tanaka T, Kubo S, Nishiguchi S. Role of vitamin $K_2$ in the development of hepatocellular carcinoma in women with viral cirrhosis of the liver. *JAMA* 2004; 292:358-61.
10. Mizuta T, Ozaki I, Eguchi Y, Yasutake T, Kawazoe S, Fujimoto K, Yamamoto K. The effect of menatetrenone, a vitamin $K_2$ analog, on disease recurrence and survival in patients with hepatocellular carcinoma after curative treatment: a pilot study. Cancer 2006; 106:867-72.
11. Yaguchi M, Miyazawa K, Otawa M, Katagiri T, Nishimaki J, Uchida Y, Iwase O, Gotoh A, Kawanishi Y, Toyama K. Vitamin K2 selectively induces apoptosis of blastic cells in myelodysplastic syndrome: Flow cytometric detection of apoptotic cells using APO2.7 monoclonal antibody. Leukemia 1998; 12:1392-7.
12. Miyazawa K, Yaguchi M, Funato K, Gotoh A, Kawanishi Y, Nishizawa Y, Yuo A, Ohyashiki K. Apoptosis/differentiation-inducing effects of vitamin K2 on HL-60 cells: dichotomous nature of vitamin K2 in leukemia cells. Leukemia 2001; 15:1111-7.
13. Nishimaki J, Miyazawa K, Yaguchi M, Katagiri T, Kawanishi Y, Toyama K, Ohyashiki K, Hashimoto S, Nakaya K, Takiguchi T. Vitamin K2 induces apoptosis of a novel cell line established from a patient with myelodysplastic syndrome in blastic transformation. Leukemia 1999; 9:1399-405.
14. Matsumoto K, Okano J, Nagahara T, Murawaki Y. Apoptosis of liver cancer cells by vitamin K2 and enhancement by MEK inhibition. Int J Oncol 2006; 29:1501-8.
15. Kanamori T, Shimizu M, Okuno M, Matsushima-Nishiwaki R, Tsurumi H, Kojima S, Moriwaki H. Synergistic growth inhibition by acyclic retinoid and vitamin K2 in human hepatocellular carcinoma cells. Cancer Sci 2007; 98:431-7.
16. Martelli AM, Zweyer M, Ochs RL, Tazzari PL, Tabellini G, Narducci P, Bortul R. Nuclear apoptotic changes: an overview. J Cell Biochem 2001; 82:634-46.
17. Green DR, Reed JC. Mitochondria and apoptosis. Science 1998; 281:1309-12.
18. Reed JC. Apoptosis-targeted therapies for cancer. Cancer Cell 2003; 3:17-22.
19. Clarke P. Developmental cell death: morphological diversity and multiple mechanisms. Anat Embryol (Berl) 1990; 181:195-213.
20. Bursch W, Ellinger A, Gerner C, Frohwein U, Schulte-Hermann R. Programmed cell death (PCD). Apoptosis, autophagic PCD, or others? Ann N Y Acad Sci 2000; 926:1-12.
21. Kondo Y, Kanzawa T, Sawaya R, Kondo S. Role of autophagy in cancer development and response to therapy. Nat Rev Cancer 2005; 5:726-34.
22. Levine B, Yuan J. Autophagy in cell death: an innocent convict? J Clin Invest 2005; 115:2679-88.
23. Klionsky D J, Emr SD. Autophagy as a regulated pathway of cellular degradation. Science 2000; 290:1717-21.
24. Yoshimori T. Autophagy: a regulated bulk degradation process inside cells. Biochem Biophysical Research Communications 2004; 313:453-8.
25. Ohsumi Y. Molecular dissection of autophagy: two ubiquitin-like systems. Nat Rev Mol Cell Biol 2001; 3:211-6.
26. Saeki K, Yuo A, Okuma E, Yazaki Y, Susin SA, Kroemer G, Takaku F. Bcl-2 downregulation causes autophagy in a caspase-independent manner in human leukemic HL60 cells. Cell Death Differ 2000; 12:1263-9.
27. Pattingre S, Tassa A, Qu X, Garuti R, Liang XH, Mizushima N, Packer M, Schneider MD, Levine B. Bcl-2 antiapoptotic proteins inhibit Beclin 1-dependent autophagy. Cell 2005; 122:927-39.
28. Pattingre S, Levine B. Bcl-2 inhibition of autophagy: A new route to cancer? Cancer Res 2006; 66:2885-8.
29. Paglin S, Hollister T, Delohery T, Hackett N, McMahill M, Sphicas E, Domingo D, Yahalom J. A novel response of cancer cells to radiation involves autophagy and formation of acidic vesicles. Cancer Res 2001; 61:439-44.
30. Kanzawa T, Kondo Y, Ito H, Kondo S, Germano I. Induction of autophagic cell death in malignant glioma cells by arsenic trioxide. Cancer Res 2003; 63:2103-8.
31. Seglen PO, Gordon PB. 3-Methyladenine: specific inhibitor of autophagic/lysosomal protein degradation in isolated rat hepatocytes. Proc Natl Acad Sci USA 1982; 79:1889-92.
32. Aoki H, Takada Y, Kondo S, Sawaya R, Aggarwal BB, Kondo Y. Evidence that curcumin suppresses the growth of malignant gliomas in vitro and in vivo through induction of autophagy: role of Akt and extracellular signal-regulated kinase signaling pathways. Mol Pharmacol 2007; 72:29-39.
33. Hosokawa N, Hara Y, Mizushima N. Genaration of cell lines with tetracycline-regulated autophagy and a role for autophagy in controlling cell size. FEBS Letters 2006; 580:2623-9.

34. Kabeya Y, Mizushima N, Ueno T, Yamamoto A, Kirisako T, Noda T, Kominami E, Ohsumi Y, Yoshimori T. LC3, a mammalian homologue of yeast Apg8p, is localized in autophagosome membranes after processing. EMBO J 2000; 19:5720-8.
35. Mizushima N. Methods for monitoring autophagy. Int J Biochem Cell Biol 2004; 36:2491-502.
36. Mizushima N, Yoshimori T. How to interpret LC3 immunoblotting. Autophagy 2007; 3:1-4.
37. Klionsky DJ, Abeliovich H, Agostinis P, et al. Guidelines for the use and interpretation of assays for monitoring autophagy in higher eukaryotes. Autophagy 2008; 4:151-75.
38. Tanida I, Minematsu-Ikeguchi N, Ueno T, Kominami E. Lysosomal turnover, but not a cellular level, of endogenous LC3 is a marker for autophagy. Autophagy 2005; 1:84-91.
39. Xue L, Fletcher GC, Tolkovsky AM. Autophagy is activated by apoptotic signalling in sympathetic neurons: an alternative mechanism of death execution. Mol Cell Neurosci 1999; 14:180-98.
40. Scott RC, Juhász G, Neufeld TP. Direct induction of autophagy by Atg1 inhibits cell growth and induces apoptotic cell death. Curr Biol 2007; 17:1-11.
41. Kanzawa T, Germano IM, Komata T, Ito H, Kondo Y, Kondo S. Role of autophagy in temozolomide-induced cytotoxicity for malignant glioma cells. Cell Death Differ 2004; 11:448-57.
42. Shao Y, Gao Z, Marks PA, Jiang X. Apoptotic and autophagic cell death induced by histone deacetylase inhibitors. Proc Natl Acad Sci USA 2004; 101:18030-5.
43. Yu L, Alva A, Su H, Dutt P, Freundt E, Welsh S, Baehrecke EH, Lenardo MJ. Regulation of an ATG7-beclin 1 program of autophagic cell death by caspase-8. Science 2004; 304:1500-2.
44. Shimizu S, Kanaseki T, Mizushima N, Mizuta T, Arakawa-Kobayashi S, Thompson CB, Tsujimoto Y. Role of Bcl-2 family proteins in a non-apoptotic programmed cell death dependent on autophagy genes. Nat Cell Biol 2004; 6:1221-8.
45. Kessel D, Reiners JJ Jr. Initiation of apoptosis and autophagy by the Bcl-2 antagonist HA14-1. Cancer Lett 2007; 249:294-9.
46. Nakayama K, Nakayama K, Negishi I, Kuida K, Sawa H, Loh DY. Targeted disruption of Bcl-2 alpha beta in mice: occurrence of gray hair, polycystic kidney disease, and lymphocytopenia. Proc Natl Acad Sci USA 1994; 91:3700-4.
47. Hoyer-Hansen M, Bastholm L, Szyniarowski P, Campanella M, Szabadkai G, Farkas T, Bianchi K, Fehrenbacher N, Elling F, Rizzuto R, Mathiasen IS, Jaattela M. Control of macroautophagy by calcium, calmodulin-dependent kinase kinase-beta, and Bcl-2. Mol Cell 2007; 25:193-205.
48. Martelli AM, Zweyer M, Ochs RL. Nuclear apoptotic changes: an overview. J Cellular Biochemistry 2001; 82:634-46.
49. Berry DL, Baehrecke EH. Growth arrest and autophagy are required for salivary gland cell degradation in Drosophila Cell 131:1137-48.
50. Yu L, Wan F, Dutta S, Welsh S, Liu Z, Freundt E, Baehrecke EH, Lenardo M. Autophagic programmed cell death by selective catalase degradation. Proc Natl Acad Sci USA 2006; 103:4952-7.
51. Qu X, Zou Z, Sun Q, Luby-Phelps K, Cheng P, Hogan RN, Gilpin C, Levine B. Autophagy gene-dependent clearance of apoptotic cells during embryonic development. Cell 2007; 128:931-46.

KTZ-1288

# Peptidoglycan and lipopolysaccharide activate PLCγ2, leading to enhanced cytokine production in macrophages and dendritic cells

**Daisuke Aki[1,2], Yasumasa Minoda[1], Hideyuki Yoshida[1], Satoko Watanabe[1], Ryoko Yoshida[1], Giichi Takaesu[1], Takatoshi Chinen[1], Toshiya Inaba[2], Masaki Hikida[3], Tomohiro Kurosaki[3], Kazuko Saeki[1] and Akihiko Yoshimura[1,*]**

[1]*Division of Molecular and Cellular Immunology, Medical Institute of Bioregulation, Kyushu University, Maidashi, Higashi-ku, Fukuoka 812-8582, Japan*

[2]*Department of Molecular Oncology and Leukemia Program Project, Research Institute for Radiation Biology and Medicine, Hiroshima University, Kasumi, Minami-ku, Hiroshima 734-8553, Japan*

[3]*Laboratory for Lymphocyte Differentiation, RIKEN Research Center for Allergy and Immunology, 1-7-22, Suehirocho, Tsurumi-ku, Yokohama, Kanagawa 230-0045, Japan*

**In macrophages and monocytes, microbial components trigger the production of pro-inflammatory cytokine through Toll-like receptors (TLRs). Although major TLR signaling pathways are mediated by serine/threonine kinases, including TAK1, IKK and MAP kinases, tyrosine phosphorylation of intracellular proteins by TLR ligands has been suggested in a number of reports. Here, we demonstrated that peptidoglycan (PGN) of a Gram-positive bacterial cell wall component, a TLR2 ligand and lipopoysaccharide (LPS) of a Gram-positive bacterial component, a TLR4 ligand induced tyrosine phosphorylation of phospholipase Cγ-2 (PLCγ2), leading to intracellular free $Ca^{2+}$ mobilization in bone marrow-derived macrophages (BMMϕ) and bone marrow-derived dendritic cells (BMDC). PGN- and LPS-induced $Ca^{2+}$ mobilization was not observed in BMDC from PLCγ2 knockout mice. Thus, PLCγ2 is essential for TLR2 and TLR4-mediated $Ca^{2+}$ flux. In PLCγ2-knockdown cells, PGN-induced IκB-α phosphorylation and p38 activation were reduced. Moreover, PLCγ2 was necessary for the full production of TNF-α and IL-6. These data indicate that the PLCγ2 pathway plays an important role in bacterial ligands-induced activation of macrophages and dendritic cells.**

## Introduction

Toll-like receptors (TLRs), which recognize the structure of microorganisms, are essential for innate immune signaling (Akira 2003; Akira *et al.* 2006). Peptidoglycan (PGN) is a major component of the cell wall of Gram-positive bacteria, and it activates the innate immune system of the host. TLR2 has been shown to be a main receptor recognizing PGN, and its activation in response to PGN induces the production of pro-inflammatory cytokines, chemokines and adhesion molecules (Akira *et al.* 2006; O'Neill & Bowie 2007). For TLR2 signaling, TLR2 utilizes adaptor proteins Myeloid differentiation 88 (MyD88) and MyD88-adaptor like (Mal) to activate IL-1 receptor-associated kinase. Then, the activated IL-1 receptor-associated kinase dissociates the MyD88/Mal complex from the receptor, followed by association with tumor necrosis factor-associated factor 6 (TRAF6). This triggers the activation of the Rel family transcription factor NF-κB, which is required for transactivation of gene expression (Akira *et al.* 2006; O'Neill *et al.* 2007). In addition, MAP kinases, including p38, JNK and ERK, are also activated in response to PGN, which leads to activation of AP-1 and ATF2 transcription factors (Chang *et al.* 2005).

In lymphocytes, $Ca^{2+}$ is important for cellular function as a second messenger (Gallo *et al.* 2006). It is generally established that ligation of antigen receptors induces the generation of inositol-1,4,5-triphospate ($IP_3$) and

*Communicated by*: Tetsuya Taga
**Correspondence*: E-mail: yakihiko@bioreg.kyushu-u.ac.jp

DOI: 10.1111/j.1365-2443.2007.01159.x

diacylglycerol (DAG). $IP_3$ binds to $IP_3R$ in the membrane of the endoplasmic reticulum (ER) and induces the release of $Ca^{2+}$ into the cytoplasm, whereas DAG, together with $Ca^{2+}$, activates protein kinase C (PKC) (Berridge 1993; Nishizuka 1995; Carpenter & Ji 1999). Recent studies suggest that the $Ca^{2+}$ flux is also activated via TLR signaling (Chun & Prince 2006; Zhou *et al.* 2006). The TLR2 ligand, $Pam_3Cys$-Ser-$Lys_4$ (P3C), stimulated the release of $Ca^{2+}$ by activating TLR2 phosphorylation by c-Src and recruited phosphatidylinositol 3-kinase (PI3K) and phospholipase Cγ (PLCγ) to affect $Ca^{2+}$ release through $IP_3$ in airway epithelial cells (Chun & Prince 2006). Furthermore, $Ca^{2+}$ release has also been shown to increase upon the stimulation of TLR4 (Zhou *et al.* 2006). However, few studies have demonstrated a direct contribution of PLCγ2 to the PGN-induced $Ca^{2+}$ mobilization. Furthermore, the importance of this pathway for pro-inflammatory cytokine production has not been elucidated.

In this study, we investigated a loss-of-function effect of PLCγ2 in PGN-stimulated macrophages and dendritic cells. PLCγ2 depletion using siRNA reduced PGN-induced p38, Akt and IκB-α phosphorylation in murine macrophage RAW 264.7 cells. Moreover, PGN and lipopolysaccharide (LPS) stimulation failed to activate TLR2- and TLR4-dependent $Ca^{2+}$ mobilization in bone marrow-derived dendritic cells (BMDC) from Tie2Cre/PLCγ2$^{flox/flox}$ mutant mice. PLCγ2 knockdown in RAW264.7 cells and knockout in bone marrow-derived macrophages (BMMφ) resulted in a reduction in the production of TNF-α, IL-6 in response to PGN. Our results indicated that $Ca^{2+}$ mobilization plays an important role in pro-inflammatory cytokine production induced by the PGN/TLR2 as well as the LPS/TLR4 pathways.

## Results

### PGN-and LPS-induced tyrosine phosphorylation of PLCγ2 in BMMφ and BMDC

Previously, we identified several tyrosine-phosphorylated proteins in LPS-activated RAW 264.7 cells using proteomic approaches. Among them, we noticed PLCγ2 (Aki *et al.* 2005). To confirm the tyrosine phosphorylation of PLCγ2 in the stimulation to LPS, we performed immunoblot analysis using an anti-phosphotyrosine (4G10) and PLCγ2 antibody in LPS-stimulated BMDC. As a result, the tyrosine phosphorylation level of PLCγ2 was increased after 30 min of LPS stimulation (Fig. 1A). Furthermore, we found that PGN, one of the bacterial ligands for TLR2, also induced tyrosine phosphorylation of PLCγ2. As shown in Fig. 1B, total cell lysates from RAW264.7 cells were isolated 0, 15, 30, 60 and 180 min after stimulation with PGN. Tyrosine-phosphorylated proteins were immunoprecipitated with 4G10 and immunoblotted with anti-PLCγ2 antibody or 4G10. Tyrosine phosphorylation of PLCγ2 increased within 30 min of PGN stimulation (Fig. 1B). To investigate whether tyrosine phosphorylation of PLCγ2 is induced in response to other TLR ligands, we examined the effects of zymosan (TLR2), Poly(I:C) (TLR3) and CpG-ODN (TLR9). As a result, tyrosine-phosphorylation of PLCγ2 was induced by zymosan as well as LPS and PGN, but Poly(I:C) and CpG-ODN which is mimic a viral infection failed to induce ligands-dependent PLCγ2 tyrosine-phosphorylation (Fig. 1C). This data indicated that PLCγ2 is induced tyrosine-phosphorylation by TLR2 and TLR4 stimulation. In addition, after pre-treatment with the tyrosine kinases inhibitor PP2 in BMMφ, PGN-induced PLCγ2 tyrosine phosphorylation was completely inhibited (Fig. 1D), suggesting that tyrosine phosphorylation of PLCγ2 is PTKs-dependent. Interestingly, PLCγ2 tyrosine phosphorylation continued for 180 min (Fig. 1B). This suggests an indirect effect of PGN on the tyrosine phosphorylation of PLCγ2. Thus, BMMφ were pre-treated with a translational inhibitor, cycloheximide for 30 min and then treated with PGN for 180 min. PGN-induced tyrosine phosphorylation of PLCγ2, as well as the tyrosine phosphorylation of the entire protein, was partially inhibited by cycloheximide (Fig. 1E). These data suggest that PLCγ2 was tyrosine-phosphorylated by direct activation of tyrosine kinases and an indirect effect, which required a new protein synthesis.

### PGN induces intracellular $Ca^{2+}$ mobilization in macrophages and dendritic cells

To examine whether TLR-ligands can induce intracellular $Ca^{2+}$ mobilization, BMMφ were loaded with Fluo-3/AM and then stimulated with PGN and their fluorescence intensity was measured using confocal microscope. A transient increase in fluorescence intensity was induced after PGN treatment (Fig. 2A). The concentration of $Ca^{2+}$ reached its maximum level within a few seconds and quickly returned to the baseline level (Fig. 2A). In BMDC, similar PGN-dependent intracellular $Ca^{2+}$ mobilization to that for BMMφ was induced (Fig. 2B). Moreover, we also observed that LPS stimulation also induced $Ca^{2+}$ mobilization in BMDC (Fig. 2C). These results indicated that bacterial ligands caused a transient increase in the concentration of $Ca^{2+}$ via TLR signaling in BMMφ and BMDC.

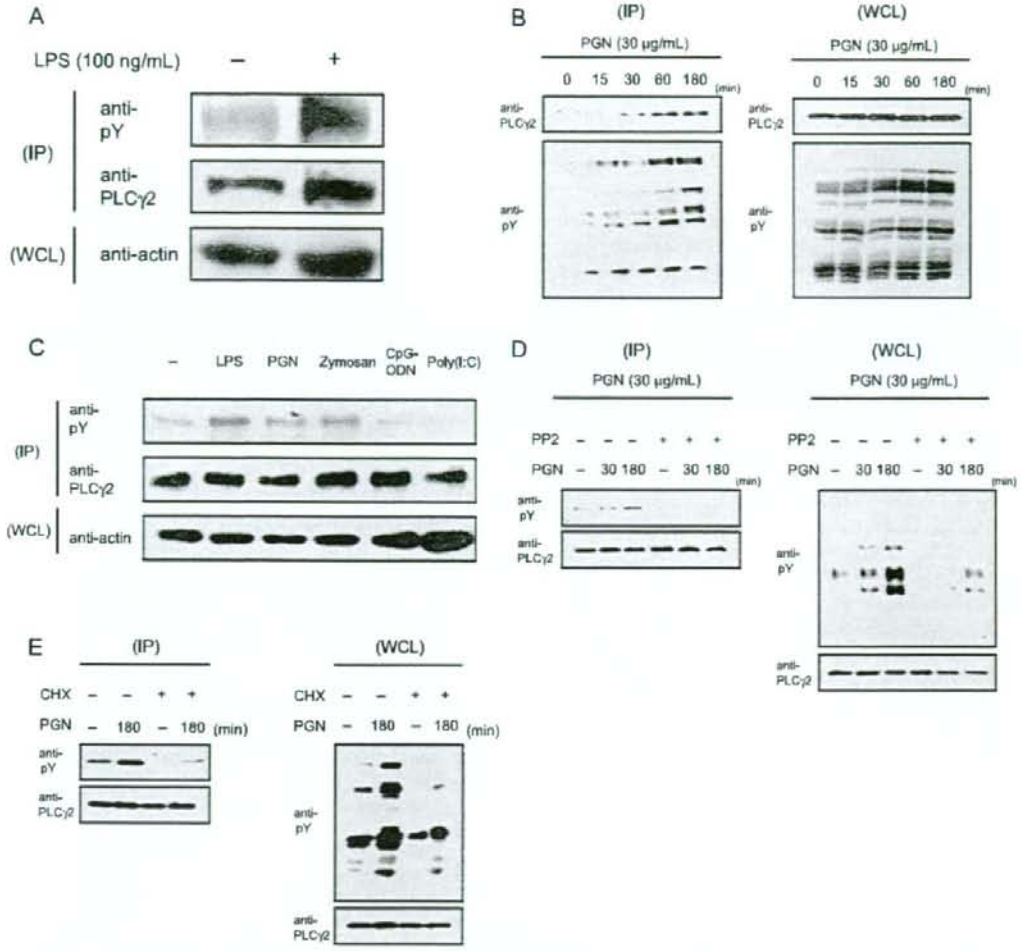


**Figure 1** TLR2 and TLR4 signaling induced tyrosine phosphorylation of PLCγ2. (A) BMDC were stimulated with 100 ng/mL LPS for 30 min. Cell extracts were immunoprecipitated with anti-PLCγ2 antibody and then immunoblotted with anti-phosphotyrosine antibody (4G10). (B) RAW264.7 cells were stimulated with 30 μg/mL PGN for the indicated time and then lysed. Cell extracts were immunoprecipitated with 4G10 and then immunoblotted with anti-PLCγ2 antibody. (C) BMMϕ were stimulated with 1 μg/mL LPS, 20 μg/mL PGN, 20 μg/mL zymosan, 1 μM CpG-ODN or 100 μg/mL Poly(I : C) for 180 min. Cell extracts were immunoprecipitated with anti-PLCγ2 antibody and then immunobloted with the indicated antibodies. (D, E) BMMϕ were pre-treated with 10 μM PP2 for 15 min (D) and 10 μM cycloheximide for 30 min (E) and then stimulated with PGN for the indicated period. Cell extracts were immunoprecipitated with anti-PLCγ2 antibody and immunoblotted with 4G10.

## PLCγ2 is required for PGN- and LPS-induced $Ca^{2+}$ signaling

The $Ca^{2+}$ flux is essential for many cellular responses. Inositol 1,4,5-triphosphate ($IP_3$) generated by PLCγ has been shown to be responsible for $Ca^{2+}$ mobilization from the ER (Berridge 1993; Nishizuka 1995; Carpenter & Ji 1999). To elucidate whether PLCγ2 is involved in $Ca^{2+}$ mobilization in response to PGN, we first assessed the effect of a PLC inhibitor, U73122, on PGN-stimulated hTLR2-expressing HEK 293 cells. U73122 pre-treatment for 30 min, but not DMSO, blocked PGN-induced

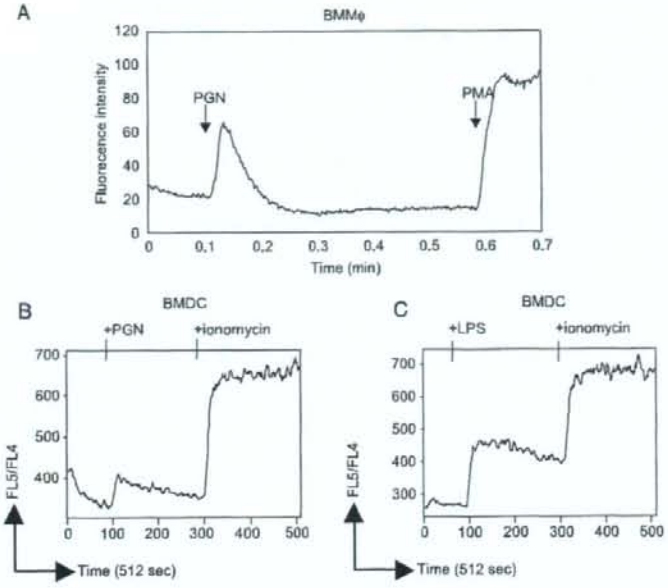


**Figure 2** TLR2 and TLR4 activate intracellular $Ca^{2+}$ mobilization in BMMφ and BMDC. (A) BMMφ were loaded with Fluo-3/AM and stimulated with 50 μg/mL PGN. (B, C) BMDC were loaded onto Indo-1 AM and then stimulated with 50 μg/mL PGN (B) or 100 ng/mL LPS (C). Intracellular $Ca^{2+}$ mobilization was evaluated as described in Experimental procedures. Sequentially, these cells were stimulated with PMA or ionomycin as positive controls. The data shown are representative of several experiments that produced similar results.

intracellular $Ca^{2+}$ mobilization (Fig. 3A). Next, to confirm the essential role of PLCγ2 in TLR-mediated intracellular $Ca^{2+}$ mobilization, we generated Tie2-Cre PLCγ2$^{flox/flox}$ mice. PLCγ2$^{flox/flox}$ mice, in which an exon encoding the phosphatidylinositol-4,5-biphosphate ($PIP_2$) binding site of the PLCγ2 gene is flanked by two loxP sites, have been described elsewhere (Hashimoto *et al.* 2000). The PLCγ2 gene was efficiently deleted in BMDC from homozygous mutant mice (Fig. 3B). We then examined the PGN-induced intracellular $Ca^{2+}$ release of BMDC from Tie2-Cre PLCγ2$^{flox/flox}$ mice. PGN-mediated $Ca^{2+}$ mobilization was completely blocked in the BMDC from mutant mice (Fig. 3C). This result was consistent with a blocking effect of U73122 on $Ca^{2+}$ mobilization in PGN-treated HEK293 cells stably expressing TLR2 (Fig. 3A). In addition, the LPS-induced transient $Ca^{2+}$ increase was also significantly inhibited in BMDC from Tie2-Cre PLCγ2$^{flox/flox}$ mutant mice (Fig. 3D). These data indicate that PLCγ2 is necessary for intracellular $Ca^{2+}$ mobilization in response to TLR stimulation in BMMφ and BMDC.

### TLR2-PLCγ2 signaling pathway is involved in PGN-induced p38, Akt, IκB-α and pro-inflammatory cytokine production

To explore the physiological role of PLCγ2 in TLR signaling, we generated RAW264.7 cells that were transfected with a vector expressing PLCγ2 siRNA. Immunoblot analysis indicated the silencing of PLCγ2 expression in RAW264.7 cells by PLCγ2 siRNA. The reduction of PLCγ2 levels by siRNA was greater in #2 than in #1 (Fig. 4A).

NF-κB, MAPK and Akt pathways are known to be the major downstream pathways in TLR signaling (Arbibe *et al.* 2000; Akira *et al.* 2006). As shown in Fig. 4B, silencing of PLCγ2 diminished the PGN-induced phosphorylation of p38, Akt and IκB-α. However, ERK phosphorylation was indistinguishable from empty vector-transfected cells (Fig. 4B). We next analyzed PGN-induced pro-inflammatory cytokines in PLCγ2 knockdown cells. PGN-induced IL-6 production from PLCγ2 knockdown cells #2 was strongly reduced. This reduction in knockdown cells #2 was due to the suppression of mRNA synthesis. Little difference was observed in PLCγ2 knockdown cells #1, where PLCγ2 level was not greatly different from that in empty vector transfected cells. TNF-α secretion was slightly inhibited in PLCγ2 knockdown cells #2; on the other hand, it was normal in knockdown cells #1 (Fig. 4C).

Finally, we found that, upon stimulation of PLCγ2$^{flox/flox}$ BMMφ with PGN, IL-6 and TNF-α production were suppressed to 50% and 37% of the control levels, respectively (Fig. 4D). Furthermore, LPS stimulation of PLCγ2$^{flox/flox}$ BMMφ inhibited cytokine production to

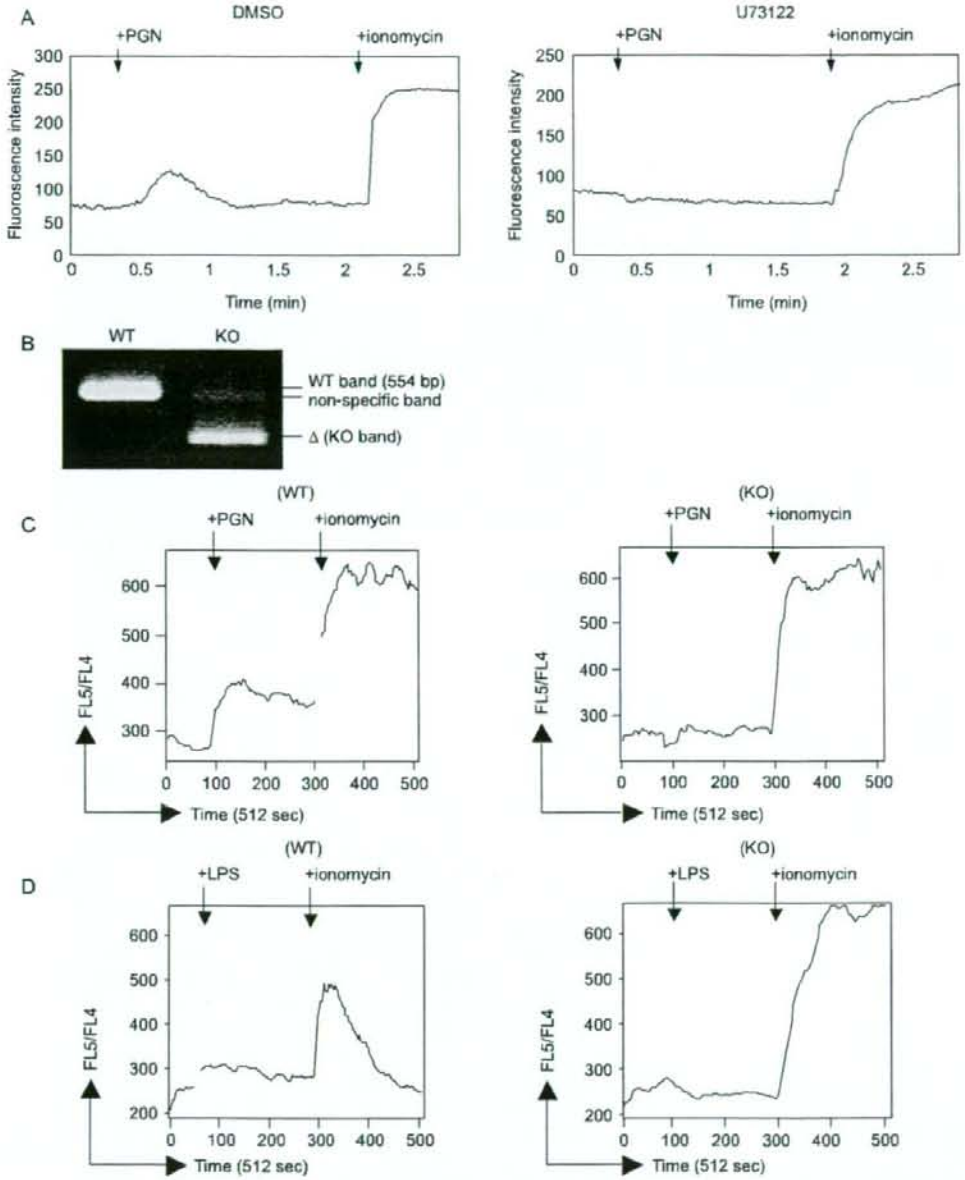


**Figure 3** PLCγ2 is essential for TLR-dependent $Ca^{2+}$ signaling. (A) HEK293 stably expressing hTLR2 cell lines were stimulated with 50 μg/mL PGN after pre-treatment with DMSO or 10 μM U73122. Cells were imaged using confocal microscope. (B) PCR analysis of genomic DNA from BMDC. The PCR product of wild-type PLCγ2 locus is 554 bp. In Tie2-Cre $PLC\gamma2^{fl/fl}$ mice, a band of 386 bp, Δ (KO band), indicates the Cre-mediated deletion of PLCγ2. (C, D) BMDC from wild-type and mutant mice stimulated with 30 μg/mL PGN (C) or 100 ng/mL LPS (D) were analyzed by flow cytometric analysis as described in Experimental procedures.

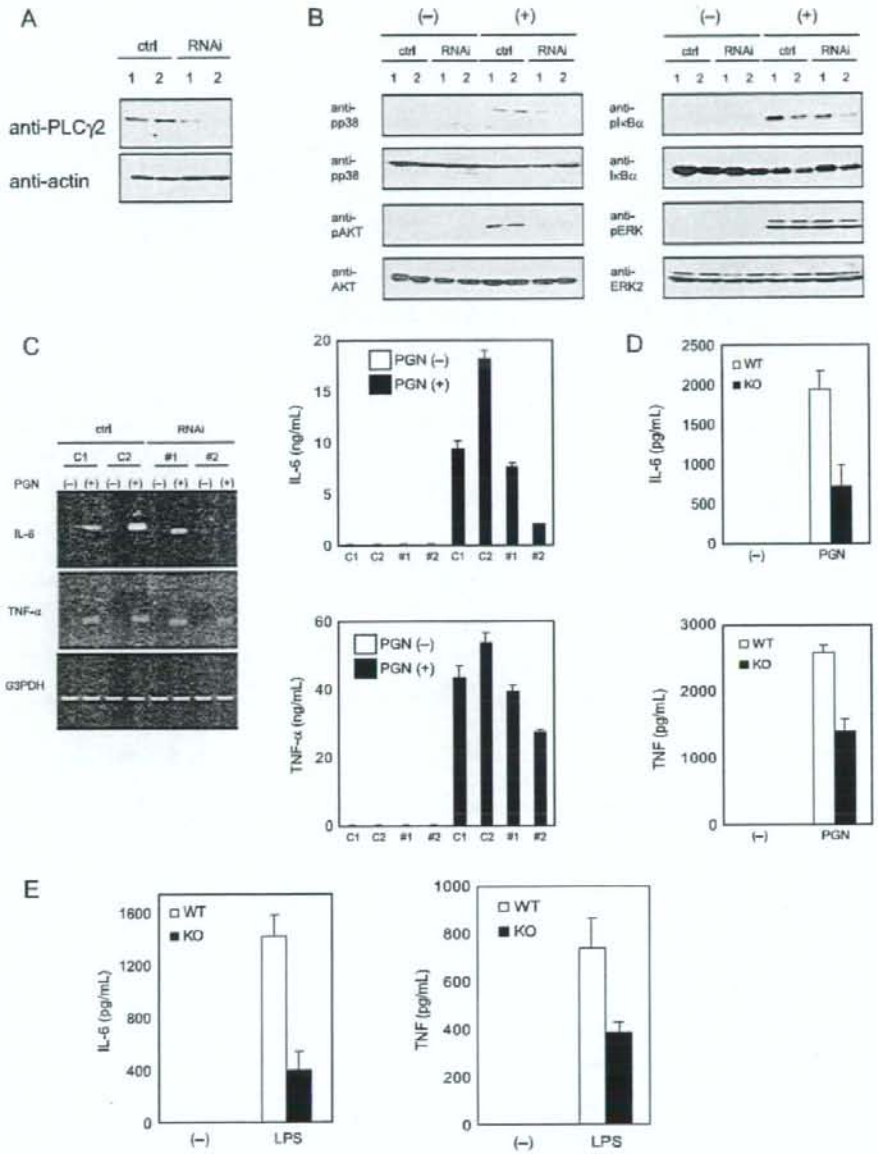


**Figure 4** PLCγ2 regulates TLR signaling and pro-inflammatory cytokine production. Two individual RAW 264.7 transformants, each containing vector alone as control or PLCγ2 siRNA expression construct, were analyzed. (A) cell extracts were immunoblotted with the indicated antibodies. (B) Transformants were stimulated with 30 μg/mL PGN. The levels of IκB-α and phospho-IκB-α were determined 15 min after stimulation. Those of p38, Akt and Erk were measured 30 min after stimulation. (C–E) For RT-PCR analysis, cells were stimulated with PGN for 1 h and then total RNA was extracted from the cells (C). For ELISA, cells were stimulated with 30 μg/mL PGN (C, D) or 100 ng/mL LPS (E) for 6 h, and IL-6 and TNF-α in the cell culture supernatants were then analyzed.

the same degree as PGN stimulation did (Fig. 4E). These data suggest that PLCγ2 is required for pro-inflammatory cytokine production mediated by PGN-and LPS-dependent $Ca^{2+}$ flux in BMMϕ and BMDC.

## Discussion

In agreement with our present study, several recent studies have demonstrated that TLRs induced rapid changes in the intracellular $Ca^{2+}$ concentration (Supajatura *et al.* 2002; Kim *et al.* 2004; Chun & Prince 2006; Zhou *et al.* 2006). $Ca^{2+}$ signaling regulates downstream signaling molecules, such as nuclear factor of activated T cells transcriptional complexes (NF-ATc) and calcineurin, followed by many cellular responses through the change of gene expression (Gallo *et al.* 2006). It has been shown that $Ca^{2+}$-dependent signaling pathway results in the gene expression of inducible nitric-oxide synthase as well as the production of TNF-α upon LPS stimulation of rat peritoneal macrophages (Zhou *et al.* 2006). Furthermore, it has been suggested that TLR-dependent PLCγ2 activation participated in this event (Shinji *et al.* 1997; Chun & Prince 2006; Zhou *et al.* 2006). However, there has been little direct evidence for the involvement of PLCγ2 in $Ca^{2+}$ mobilization in response to TLR ligands. In the present study, we found that PGN and LPS stimulation induced PLCγ2 phosphorylation and intracellular $Ca^{2+}$ mobilization in BMMϕ and BMDC. We clearly demonstrated that this pathway played an important role in the activation of macrophages using PLCγ2 knockdown cells and BMMϕ from PLCγ2-disrupted mice. Thus, it is now clear that PLCγ2 plays an important role in TLR2 and TLR4-mediated $Ca^{2+}$ mobilization and signal transduction.

There are several important questions still to be solved. First, the manner in which TLR2 and TLR4 signaling is activated is not exactly clear. TLR2-dependent PLCγ2 tyrosine phosphorylation was clearly detected at 30 min after PGN stimulation, and tyrosine phosphorylation seemed to be amplified at 180 min. Tyrosine phosphorylation of PLCγ2 at this point was not fully inhibited by cycloheximide pre-treatment; thus, there seem to be both direct and indirect pathways for PLCγ2 tyrosine phosphorylation by PGN stimulation. When PP2 was used, the phosphorylation of PLCγ2 induced by PGN was completely inhibited. This result suggested that Src family tyrosine kinases are directly involved in TLR2 signaling, as previously reported (Chun & Prince 2006). Other tyrosine kinases were required for the activation of TLR2 signaling. In particular, Syk kinase was considered to be involved in TLR2 signaling. Syk-deficient dendritic cells were unable to produce IL-2 and IL-10. In addition, Syk binds to the phosphorylation YxxL motif of the β-glucan receptor, Dectin-1, upon ligand binding. It is, therefore, suggested that Syk is recruited to the Dectin-1 phosphorylation site and participates in TLR2 signaling events (Rogers *et al.* 2005). Moreover, recent studies have demonstrated that a member of Tec family tyrosine kinase, Btk has important implications for TLR signal transduction. It has been demonstrated that Btk tyrosine phosphorylation was TLR2-dependent and the lack of Btk resulted in lower amounts of TNF-α and IL-1β production (Jefferies *et al.* 2003; Horwood *et al.* 2006). However, the question of how these tyrosine kinases are activated by PGN is unanswered. In addition, the question of how these kinases phosphorylate PLCγ2 is still not very clear.

Second, an important question is how downstream PLCγ2 is involved in TLR signaling. Apparently, the activation of PLCγ2 results in an increase of intracellular $Ca^{2+}$ and DAG. $Ca^{2+}$ activates NF-AT transcription factors, while DAG activates PKC. PKCα/β has been shown to participate in NF-κB activation upon LPS stimulation of macrophages (Asehnoune *et al.* 2005; Zhou *et al.* 2006). Cyclosporine, an inhibitor of $Ca^{2+}$-dependent NF-AT activation, has been shown to block cytokine production (Duperrier *et al.* 2002; Chen *et al.* 2004). Thus, both the $Ca^{2+}$-NFAT and the DAG-PKC pathways seem to be important for the downstream of PLCγ2 activated by TLRs. However, the precise role of NF-AT and PKC in cytokine production remains to be clarified. Furthermore, it has been shown that another PKC isoform, PKCε, is also involved in LPS signaling (Shapira *et al.* 1997; Valledor *et al.* 2000; Castrillo *et al.* 2001; McGettrick *et al.* 2006). However, it has not been clarified which PKCs isoform was activated by TLR2-PLCγ2 pathway.

The knockdown of PLCγ2 is effective enough to inhibit Akt activation in particular. The pathway for Akt activation in response to TLR ligands has not been clarified. We found that Akt activation was reduced in not only PLCγ2-knockdown cells, but also U73122 treated RAW264.7 cells (data not shown). Thus, our data raise an interesting possibility that PLCγ2 is an upstream of PI3kinase-Akt. On the other side, the generation of $PIP_3$ by PI3K also activates PLCγ2 (Bae *et al.* 1998). A recent study demonstrated that phosphorylated PLCγ1 interacted with Akt in response to EGF stimulation (Wang *et al.* 2006). Thus, Akt could be a downstream target of PLCγ2. We have shown that the suppression of PLCγ2 resulted in the reduction of IκB-α, p38 phosphorylation as well as Akt. The mechanism underlying these suppressions has not been clarified. It has been demonstrated that the PKC-CARD pathway is critical for NF-κB activation in response to T cell receptor ligation (Hara

*et al.* 2004). Several reports indicate that PKC is important for TLR signaling and cytokine production in macrophages (Chen *et al.* 1998; Castrillo *et al.* 2001; Zhou *et al.* 2006). However, the contribution of this pathway has not been clarified because NF-κB is strongly activated by the TRAF6-TAK1-IKK pathways. Furthermore, it is not known which pathway, $Ca^{2+}$ or PKC, directly regulates p38 or Akt. Further study is necessary to define the link between PLCγ2 and these pathways.

## Experimental procedures

### Antibodies and reagent

Peptidoglycan (PGN) from *Staphylococcus aureus* was purchased from Fluka (Bachs, Sweden). PP2, cyclohexamide and wortmannin were from Calbiochem (San Diego, CA). LPS, CpG-ODN and Poly(I : C) were from Sigma-Aldrich (Seelze, Germany). Zymosan was obtained from Invitrogen (Carlsbad, CA). Antibodies against PLCγ2 (Q-20), IκB-α (C-21) and ERK2 (C-14) were from Santa Cruz Biotechnology (Santa Cruz, CA). The anti-actin rabbit polyclonal antibody was purchased from Sigma (St. Louis, MO). Antibodies against Akt, p38, phospho-IκBα, phospho-p40/p42 MAP kinase, phospho-p38, phospho-Akt and 4G10 have been described (Aki *et al.* 2005).

### Mice

$PLC\gamma2^{flox/flox}$ mice and Tie2-cre transgenic mice have been previously established (Hashimoto *et al.* 2000; Kimura *et al.* 2004; Matsumura *et al.* 2007). Tie2-cre transgenic mice were bred with $PLC\gamma2^{flox/flox}$ mice to generate mice in which PLCγ2 was deleted in hemopoietic cells. All experiments were approved by the Animal Ethics Committee of Kyushu University.

### Cell culture

TLR2 stably expressing HEK293 cells were prepared by transfection of hTLR2 cDNA and selected in the presence of G418. TLR2-HEK293 cells and the murine macrophage cell line RAW264.7 cells were cultured in DMEM supplemented with 10% fetal calf serum. To prepare BMMϕ, bone marrow cells were obtained from femora and tibia of 6–8-week-old C57BL6/J mice and then cultured in RPMI 1640 medium supplemented with 10% fetal bovine serum; the culture medium was conditioned by the L929 cells containing a macrophage colony-stimulating factor (M-CSF). After 7 days, the cells were used as BMMϕ for the experiments. BMDC were prepared as described elsewhere (Matsumura *et al.* 2007).

### Immunoprecipitation and immunoblotting analysis

After stimulation, cells were washed with PBS and solubilized for 30 min at 4 °C in lysis buffer (Aki *et al.* 2005). Cell extracts were then centrifuged, and supernatants were used for immunoprecipitation with specific antibodies. After separation by SDS-PAGE and transfer to polyvinyliden difluoride membranes, proteins were analyzed by immunoblotting with the indicated antibodies.

### Measurement of cytokine

The cells were plated on 6-well plates on the day before PGN stimulation. For ELISA, the cells were stimulated with PGN for 6 h. Then, culture supernatants were collected and analyzed for TNF-α and IL-6 (BD Biosciences PharMingen, San Diego, CA). For the analysis of mRNA expression, the cells were stimulated with PGN for 1 h. TNF-α and IL-6 RT-PCR were carried out as described (Aki *et al.* 2005; Chinen *et al.* 2006).

### RNA interference

The small interfering RNA sequence that targets mouse PLCγ2 was at positions 1017–1037 (5′-GTCCTCCACGGAAGCG-TATAT-3′). The annealed oligonucleotides were inserted into psiRNA-hH1neo expression vector (InvivoGen, San Diego, CA). Stable transformants were selected in 1 mg/mL G418.

### $Ca^{2+}$ flux analysis

For imaging, cells were grown in coverglass chamberslides and loaded for 30 min at 37 °C with 5 μM Fluo3/AM (DOJINDO) in the dark. Cells were washed with HANKS buffer. Fluorescence imaging was obtained using Carl Zeiss LSM 510 META scanning confocal microscope and analyzed using LSM Image Browse. For flow cytometric analysis, $1.0 \times 10^7$ BMDC cells were suspended in 10 mL of RPMI medium supplemented and loaded with 3 μM Indo-1 AM (Molecular Probes, Eugene, OR) at 37 °C for 30 min. After washing, $1.0 \times 10^6$ cells were used for analysis. The filter set-up on the BD LSR for Indo-1 was FL-5 424/444 nm BF filter and unbound Indo-1 FL-4 530/530 nm BF filter. The $Ca^{2+}$ flux was measured as the ratio between the calcium bound Indo-1 and unbound or FL-5/FL-4 vs. time. Full-scale deflection of the $Ca^{2+}$ flux was measured by the addition of 3.0 μg/mL ionomycin.

## Acknowledgements

We thank Dr T. Muta (University of Tohoku) for hTLR2 cDNAs, Ms T. Yoshioka and M. Ohtsu for technical assistance, and Ms Y. Nishi for manuscript preparation. This study was supported by special Grants-in-Aid from the Ministry of Education, Culture, Sports, Science, and Technology of Japan, the Program for Promotion of Fundamental Studies in Health Sciences of the National Institute of Biomedical Innovation (NIBIO), the Naito Memorial Foundation, the Takeda Science Foundation, the Mochida Memorial Foundation, the Kato Memorial Foundation, the Kanae Foundation for the promotion of Medical Science, Clinical Research Foundation, the Osaka Cancer research Foundation, Mitsubishi Pharma Research Foundation and the Ichiro Kanehara Memorial Foundation.

## References


Aki, D., Mashima, R., Saeki, K., Minoda, Y., Yamauchi, M. & Yoshimura, A. (2005) Modulation of TLR signalling by the C-terminal Src kinase (Csk) in macrophages. *Genes Cells* **10**, 357–368.

Akira, S. (2003) Toll-like receptor signaling. *J. Biol. Chem.* **278**, 38105–38108.

Akira, S., Uematsu, S. & Takeuchi, O. (2006) Pathogen recognition and innate immunity. *Cell* **124**, 783–801.

Arbibe, L., Mira, J.P., Teusch, N., Kline, L., Guha, M., Mackman, N., Godowski, P.J., Ulevitch, R.J. & Knaus, U.G. (2000) Toll-like receptor 2-mediated NF-κB activation requires a Rac1-dependent pathway. *Nat. Immunol.* **1**, 533–540.

Asehnoune, K., Strassheim, D., Mitra, S., Yeol Kim, J. & Abraham, E. (2005) Involvement of PKCα/β in TLR4 and TLR2 dependent activation of NF-κB. *Cell. Signal.* **17**, 385–394.

Bae, Y.S., Cantley, L.G., Chen, C.S., Kim, S.R., Kwon, K.S. & Rhee, S.G. (1998) Activation of phospholipase C-γ by phosphatidylinositol 3,4,5-trisphosphate. *J. Biol. Chem.* **273**, 4465–4469.

Berridge, M.J. (1993) Inositol trisphosphate and calcium signalling. *Nature* **361**, 315–325.

Carpenter, G. & Ji, Q. (1999) Phospholipase C-γ as a signal-transducing element. *Exp. Cell Res.* **253**, 15–24.

Castrillo, A., Pennington, D.J., Otto, F., Parker, P.J., Owen, M.J. & Bosca, L. (2001) Protein kinase Cepsilon is required for macrophage activation and defense against bacterial infection. *J. Exp. Med.* **194**, 1231–1242.

Chang, Y.J., Wu, M.S., Lin, J.T. & Chen, C.C. (2005) Helicobacter pylori-Induced invasion and angiogenesis of gastric cells is mediated by cyclooxygenase-2 induction through TLR2/TLR9 and promoter regulation. *J. Immunol.* **175**, 8242–8252.

Chen, C.C., Wang, J.K. & Lin, S.B. (1998) Antisense oligonucleotides targeting protein kinase C-α,-βI, or -δ but not -η inhibit lipopolysaccharide-induced nitric oxide synthase expression in RAW 264.7 macrophages: involvement of a nuclear factor κB-dependent mechanism. *J. Immunol.* **161**, 6206–6214.

Chen, T., Guo, J., Yang, M., Han, C., Zhang, M., Chen, W., Liu, Q., Wang, J. & Cao, X. (2004) Cyclosporin A impairs dendritic cell migration by regulating chemokine receptor expression and inhibiting cyclooxygenase-2 expression. *Blood* **103**, 413–421.

Chinen, T., Kobayashi, T., Ogata, H., Takaesu, G., Takaki, H., Hashimoto, M., Yagita, H., Nawata, H. & Yoshimura, A. (2006) Suppressor of cytokine signaling-1 regulates inflammatory bowel disease in which both IFNγ and IL-4 are involved. *Gastroenterology* **130**, 373–388.

Chun, J. & Prince, A. (2006) Activation of $Ca^{2+}$-dependent signaling by TLR2. *J. Immunol.* **177**, 1330–1337.

Duperrier, K., Farre, A., Bienvenu, J., Bleyzac, N., Bernaud, J., Gebuhrer, L., Rigal, D. & Eljaafari, A. (2002) Cyclosporin A inhibits dendritic cell maturation promoted by TNF-α or LPS but not by double-stranded RNA or CD40L. *J. Leukoc. Biol.* **72**, 953–961.

Gallo, E.M., Cante-Barrett, K. & Crabtree, G.R. (2006) Lymphocyte calcium signaling from membrane to nucleus. *Nat. Immunol.* **7**, 25–32.

Hara, H., Bakal, C., Wada, T., Bouchard, D., Rottapel, R., Saito, T. & Penninger, J.M. (2004) The molecular adapter Carma1 controls entry of IκB kinase into the central immune synapse. *J. Exp. Med.* **200**, 167–177.

Hashimoto, A., Takeda, K., Inaba, M., Sekimata, M., Kaisho, T., Ikehara, S., Homma, Y., Akira, S. & Kurosaki, T. (2000) Cutting edge: essential role of phospholipase C-γ2 in B cell development and function. *J. Immunol.* **165**, 1738–1742.

Horwood, N.J., Page, T.H., McDaid, J.P., Palmer, C.D., Campbell, J., Mahon, T., Brennan, F.M., Webster, D. & Foxwell, B.M. (2006) Bruton's tyrosine kinase is required for TLR2 and TLR4-induced TNF, but not IL-6, production. *J. Immunol.* **176**, 3635–3641.

Jefferies, C.A., Doyle, S., Brunner, C., Dunne, A., Brint, E., Wietek, C., Walch, E., Wirth, T. & O'Neill, L.A. (2003) Bruton's tyrosine kinase is a Toll/interleukin-1 receptor domain-binding protein that participates in nuclear factor κB activation by Toll-like receptor 4. *J. Biol. Chem.* **278**, 26258–26264.

Kim, Y., Moon, J.S., Lee, K.S., Park, S.Y., Cheong, J., Kang, H.S., Lee, H.Y. & Kim, H.D. (2004) $Ca^{2+}$/calmodulin-dependent protein phosphatase calcineurin mediates the expression of iNOS through IKK and NF-κB activity in LPS-stimulated mouse peritoneal macrophages and RAW 264.7 cells. *Biochem. Biophys. Res. Commun.* **314**, 695–703.

Kimura, A., Kinjyo, I., Matsumura, Y., Mori, H., Mashima, R., Harada, M., Chien, K.R., Yasukawa, H. & Yoshimura, A. (2004) SOCS3 is a physiological negative regulator for granulopoiesis and granulocyte colony-stimulating factor receptor signaling. *J. Biol. Chem.* **279**, 6905–6910.

Matsumura, Y., Kobayashi, T., Ichiyama, K., Yoshida, R., Hashimoto, M., Takimoto, T., Tanaka, K., Chinen, T., Shichita, T., Wyss-Coray, T., Sato, K. & Yoshimura, A. (2007) Selective expansion of foxp3-positive regulatory T cells and immunosuppression by suppressors of cytokine signaling 3-deficient dendritic cells. *J. Immunol.* **179**, 2170–2179.

McGettrick, A.F., Brint, E.K., Palsson-McDermott, E.M., Rowe, D.C., Golenbock, D.T., Gay, N.J., Fitzgerald, K.A. & O'Neill, L.A. (2006) Trif-related adapter molecule is phosphorylated by PKCε during Toll-like receptor 4 signaling. *Proc. Natl. Acad. Sci. USA* **103**, 9196–9201.

Nishizuka, Y. (1995) Protein kinase C and lipid signaling for sustained cellular responses. *FASEB J.* **9**, 9484–9496.

O'Neill, L.A. & Bowie, A.G. (2007) The family of five: TIR-domain-containing adaptors in Toll-like receptor signalling. *Nat. Rev. Immunol.* **7**, 353–364.

Rogers, N.C., Slack, E.C., Edwards, A.D., Nolte, M.A., Schulz, O., Schweighoffer, E., Williams, D.L., Gordon, S., Tybulewicz, V.L., Brown, G.D. & Reis e Sousa, C. (2005) Syk-dependent cytokine induction by Dectin-1 reveals a novel pattern recognition pathway for C type lectins. *Immunity* **22**, 507–517.

Shapira, L., Sylvia, V.L., Halabi, A., Soskolne, W.A., Van Dyke, T.E., Dean, D.D., Boyan, B.D. & Schwartz, Z. (1997) Bacterial lipopolysaccharide induces early and late activation of protein kinase C in inflammatory macrophages by selective activation of PKC-ε. *Biochem. Biophys. Res. Commun.* **240**, 629–634.

Shinji, H., Akagawa, K.S., Tsuji, M., Maeda, M., Yamada, R., Matsuura, K., Yamamoto, S. & Yoshida, T. (1997) Lipopolysaccharide-induced biphasic inositol 1,4,5-trisphosphate response and tyrosine phosphorylation of 140-kilodalton protein in mouse peritoneal macrophages. *J. Immunol.* **158**, 1370–1376.

Supajatura, V., Ushio, H., Nakao, A., Akira, S., Okumura, K., Ra, C. & Ogawa, H. (2002) Differential responses of mast cell Toll-like receptors 2 and 4 in allergy and innate immunity. *J. Clin. Invest.* **109**, 1351–1359.

Valledor, A.F., Xaus, J., Comalada, M., Soler, C. & Celada, A. (2000) Protein kinase Cε is required for the induction of mitogen-activated protein kinase phosphatase-1 in lipopolysaccharide-stimulated macrophages. *J. Immunol.* **164**, 29–37.

Wang, Y., Wu J. & Wang, Z. (2006) Akt binds to and phosphorylates phospholipase C-γ1 in response to epidermal growth factor. *Mol. Biol. Cell* **17**, 2267–2277.

Zhou, X., Yang, W. & Li, J. (2006) $Ca^{2+}$- and protein kinase C-dependent signaling pathway for nuclear factor-κB activation, inducible nitric-oxide synthase expression, and tumor necrosis factor-α production in lipopolysaccharide-stimulated rat peritoneal macrophages. *J. Biol. Chem.* **281**, 31337–31347.

*Received*: 3 September 2007
*Accepted*: 15 November 2007

# *AML1* mutations induced MDS and MDS/AML in a mouse BMT model

Naoko Watanabe-Okochi,[1] Jiro Kitaura,[1] Ryoichi Ono,[1] Hironori Harada,[2] Yuka Harada,[3] Yukiko Komeno,[1] Hideaki Nakajima,[1] Tetsuya Nosaka,[1] Toshiya Inaba,[4] and Toshio Kitamura[1]

[1]Division of Cellular Therapy, Advanced Clinical Research Center, The Institute of Medical Science, The University of Tokyo, Tokyo; [2]Department of Hematology and Oncology, Research Institute for Radiation Biology and Medicine, Hiroshima University, Hiroshima; [3]International Radiation Information Center, Research Institute for Radiation Biology and Medicine, Hiroshima University, Hiroshima; and [4]Department of Molecular Oncology, Research Institute for Radiation Biology and Medicine, Hiroshima University, Hiroshima, Japan

**Myelodysplastic syndrome (MDS) is a hematopoietic stem-cell disorder characterized by trilineage dysplasia and susceptibility to acute myelogenous leukemia (AML). Analysis of molecular basis of MDS has been hampered by the heterogeneity of the disease. Recently, mutations of the transcription factor AML1/RUNX1 have been identified in 15% to 40% of MDS–refractory anemia with excess of blasts (RAEB) and MDS/AML. We performed mouse bone marrow transplantation (BMT) using bone marrow cells transduced with the *AML1* mutants. Most mice developed MDS and MDS/AML-like symptoms within 4 to 13 months after BMT. Interestingly, among integration sites identified, Evi1 seemed to collaborate with an *AML1* mutant harboring a point mutation in the Runt homology domain (D171N) to induce MDS/AML with an identical phenotype characterized by marked hepatosplenomegaly, myeloid dysplasia, leukocytosis, and biphenotypic surface markers. Collaboration between AML1-D171N and *Evi1* was confirmed by a BMT model where coexpression of AML1-D171N and *Evi1* induced acute leukemia of the same phenotype with much shorter latencies. On the other hand, a C-terminal truncated *AML1* mutant (S291fsX300) induced pancytopenia with erythroid dysplasia in transplanted mice, followed by progression to MDS-RAEB or MDS/AML. Thus, we have developed a useful mouse model of MDS/AML that should help in the understanding of the molecular basis of MDS and the progression of MDS to overt leukemia. (Blood. 2008;111:4297-4308)**



## Introduction

Myelodysplastic syndromes (MDS) are a heterogeneous group of clonal stem-cell disorders characterized by ineffective hematopoiesis and susceptibility to leukemic transformation (MDS/acute myelogenous leukemia [AML]). Progression from MDS-refractory anemia with excess blasts (MDS-RAEB) to AML is frequently observed in the clinical course, which is thought to result from serial acquisition of cytogenetic abnormalities.[1-5] According to the 2-hit model of leukemogenesis, one class of mutations (class I), including FLT3-ITD, N-Ras, or K-Ras mutations, confers on cells a proliferative advantage; a second class of mutations (class II), including AML1/ETO, PML/RARα, or MLL-related fusion genes, interferes with hematopoietic differentiation.[6] Indeed, it has been reported that a combination of class I and II mutations such as FLT3-ITD plus AML1-ETO or MLL-SEPT6 induced AML in a mouse bone marrow transplantation (BMT) model, while either class I or II mutations alone led to, if anything, myeloproliferative disorders (MPDs), not leukemia.[6-13] On the other hand, the precise molecular mechanism underlying development of MDS and MDS/AML remains elusive partly because there are only a few mouse models for MDS and MDS/AML available. So far, 2 distinct models of MDS have been reported: *Evi1* induced MDS-like symptoms in a mouse BMT model in which the mice succumbed to fatal peripheral cytopenia,[14] while NUP98-HOXD13 transgenic mice developed MDS and died of either various types of acute leukemia or severe anemia and leukocytopenia.[15] In the present study, we generated a mouse BMT model of MDS-RAEB and MDS/AML induced by *AML1* mutants frequently found in patients with MDS and MDS/AML. Interestingly, the phenotypes of these mice very much resemble those of the human diseases.

The *AML1* gene is located on chromosome 21q22 and is the most frequent target for chromosomal translocation in leukemia. Analysis of AML1-deficient mice has shown that *AML1* is indispensable for the establishment of definitive hematopoiesis.[16-18] As accumulated studies have demonstrated, heterozygous germline mutations in the *AML1* gene caused familial platelet disorder with predisposition to AML (FPD/AML),[19,20] and sporadic point mutations were frequently found in the development of leukemia: 21% of AML M0, 15.0% to 15.9% of MDS-RAEB and MDS/AML, and 46% of radiation-associated MDS.[21-29] The vast majority of AML1 mutations were located in the Runt homology domain (RHD), which mediated its ability to bind to DNA and core-binding factor β (CBFβ). To confirm the involvement of *AML1* mutations in hematopoietic disorders, we selected 2 types of *AML1* mutants found in patients with MDS/AML: one with a point mutation in RHD (AML1-D171N), and the other with C-terminal truncation caused by a frame-shift (AML1-S291fsX300). After transplantation using bone marrow cells infected with retrovirus vectors harboring *AML1* mutants, most of the mice that received transplants died of MDS-RAEB and MDS/AML. Long-term analysis demonstrated that the phenotype of the mice that underwent

Submitted January 15, 2007; accepted December 24, 2007. Prepublished online as *Blood* First Edition paper, January 11, 2008; DOI 10.1182/blood-2007-01-068346.

An Inside *Blood* analysis of this article appears at the front of this issue.

The online version of this article contains a data supplement.

The publication costs of this article were defrayed in part by page charge payment. Therefore, and solely to indicate this fact, this article is hereby marked "advertisement" in accordance with 18 USC section 1734.